Breakdown of linear response theory under low-power excitation in NMR. II. The case of “long-lived” signals in homogeneously broadened dipolar spin systems

Zhaoyuan Gong, and Jamie D. Walls

Citation: J. Chem. Phys. **149**, 234203 (2018); doi: 10.1063/1.5036753

THE JOURNAL OF CHEMICAL PHYSICS **149**, 234203 (2018)

Breakdown of linear response theory under low-power excitation in NMR. II. The case of “long-lived” signals in homogeneously broadened dipolar spin systems

Zhaoyuan Gong and Jamie D. Walls[a]
Department of Chemistry, University of Miami, Coral Gables, Florida 33124, USA

(Received 18 April 2018; accepted 19 November 2018; published online 21 December 2018)

In this work, the previous linear response theory developed to describe low-power, radiofrequency (RF) excitation in inhomogeneously broadened spin systems [Z. Gong and J. D. Walls, J. Chem. Phys. **145**, 164201 (2016)] is applied to the problem of low-power excitation in homogeneously broadened dipolar spin systems when the strength of the RF pulse, ν_{RF}, is much less than the homogeneous linewidth, $\Delta\nu_{\frac{1}{2}}$. Application of a low-power pulse for a time T_p with a nominal flip-angle of Θ generates a broad signal with a “dip” at the RF transmitter frequency that deepens with increasing Θ. When a delay is placed before signal acquisition, only a negative, “long-lived” signal from the narrow “dip” remains. If a π_X-pulse is applied after low-power excitation, a “long-lived” signal lasting a time $t \approx T_p$ after the π_X-pulse is generated where dephasing due to B_0 inhomogeneity, anisotropic bulk magnetic susceptibility, and chemical shift anisotropy is refocused while dephasing due to nonzero chemical shift differences is only partially refocused. Contrary to previous observations, experiments in powdered hexamethylbenzene demonstrate that these “long-lived” signals can exist even in the absence of nonzero chemical shift differences. Additional experimental demonstrations in powdered and single-crystalline adamantane and ferrocene samples are also presented. *Published by AIP Publishing.* https://doi.org/10.1063/1.5036753

I. INTRODUCTION

In an inhomogeneously broadened spin system, application of a radiofrequency (RF) pulse of strength ν_{RF} can effectively “burn a hole” when ν_{RF} is much less than the inhomogeneous linewidth,[1–4] $\Delta\nu_{\frac{1}{2}}$. Under conditions of complete saturation, the resulting spectrum after application of a low-power pulse (LPP) contains a “hole” at frequencies $|\nu| \leq \nu_{RF}$. For homogeneously broadened systems, such as dipolar solids, application of a low-power RF pulse does not burn a “hole” but instead results in overall signal attenuation. This difference in homogeneous vs. inhomogeneous broadening is attributed to differences in the underlying complexity of the system’s spin interactions. For inhomogeneously broadened systems, only a few states are connected by an applied pulse; therefore, low-power RF saturation attenuates the spectral intensity associated with only a small number of transitions. For homogeneously broadened systems, on the other hand, there exists a high degree of connectivity between states under an RF pulse that results in the RF saturation diffusing amongst many connected transitions thereby leading to an almost uniform decrease in spectral intensity. Due to the complexity of the spin dynamics in homogeneously broadened systems, a thermodynamic[5,6] picture has been developed that has successfully described the spin dynamics under continuous and pulsed spin-locking conditions. However, a corresponding spin thermodynamics picture for RF excitation and/or “hole-burning” has not been developed.

Recent experiments have examined low-power excitation in homogeneously broadened systems.[7–11] Application of a low-power RF pulse was shown to generate a narrow, negative signal that was reminiscent of “hole-burning” in inhomogeneously broadened systems. Khitrin[9,10] also demonstrated that application of a π_X-pulse directly after low-power excitation resulted in increased spectral intensity. Since a π_X-pulse does not refocus dipolar dephasing but does refocus inhomogeneous dephasing due to chemical shifts, B_0 inhomogeneity, chemical shift anisotropy (CSA), and anisotropic bulk magnetic susceptibility (ABMS),[12,13] Khitrin argued that the enhanced signal after low-power excitation followed by a π_X-pulse was a new type of spin echo generated by the non-commutivity of dipolar and chemical shift evolution between spins with nonzero chemical shift differences. It was therefore proposed that a requirement for the existence of this new type of echo under low-power RF excitation was nonzero chemical shift differences between spins.[9–11]

In this work, we apply our recent theory of low-power excitation of inhomogeneously broadened spin systems[14] to the case of low-power excitation in dipolar solids. We demonstrate that low-power excitation generates a broad spectrum, often wider than a pulse-acquire spectrum with a “dip” occurring at the RF transmitter frequency. The “dip” generated by the low-power excitation increases with increasing nominal flip-angle, Θ, which for a constant RF pulse shape of length T_p is given by $\Theta = 2\pi\nu_{RF}T_p$. If the acquisition is delayed after low-power excitation, only a “long-lived,” narrow

---

[a] Author to whom correspondence should be addressed: jwalls@miami.edu

and negative signal from the "dip" remains. According to the theory presented in this work, the "long-lived" signal is not a result of any increase in the intrinsic T_2 of the sample but rather a spectral interference phenomenon[15] whereby the broad components of the spectrum dephase leaving only the "long-lived" signal associated with the "dip" generated by the low-power excitation pulse. When a π_X-pulse is applied directly after low-power excitation, a "long-lived" signal lasting a time $t \approx T_p$ is generated whereby dephasing due to ABMS, CSA, and/or B_0 inhomogeneity is refocused while dephasing due to nonzero chemical shift differences is only partially refocused. Unlike previous reports,[10] a signal was observed in powdered hexamethylbenzene under low-power excitation followed by a π_X-pulse, which demonstrated that nonzero chemical shift differences are not required to observe such "long-lived" signals in solids. Additional experiments in powdered and single-crystalline adamantane and ferrocene samples suggest that under low-power excitation, application of a π_X-pulse mainly refocuses inhomogeneous dephasing due to CSA, ABMS, and/or B_0 inhomogeneity.

This paper is organized as follows: in Sec. II, the basic theory for low-power excitation in dipolar solids is presented along with numerical simulations. In Sec. III, experimental details are presented, followed by a discussion and comparison of the experimental results in Sec. IV with the theoretical and numerical predictions presented in Sec. II. Finally, it is shown in Appendix A that the signal from a homogeneously broadened system can always be described in terms of the signal from an inhomogeneously broadened system with a (possibly complex) frequency distribution function, $g(\omega)$, in addition to some mathematical proofs presented in Appendix B.

II. THEORY

A. Linear response results for RF excitation under homogeneous dipolar broadening

We begin by applying the linear response (LR) theory[14] developed for low-power excitation of inhomogeneously broadened systems to a system of N_s spins ($I = \frac{1}{2}$) interacting via the homonuclear dipolar interaction in the presence of a large static magnetic field applied along the $\widehat{z}$-direction, $\vec{B} = B_0\widehat{z}$. The Hamiltonian in the rotating frame (defined by the transmitter frequency ω_{tr}) is given by

$$\widehat{H}_0 = \widehat{H}_{cs} + \widehat{H}_{\text{offset}} + \widehat{H}_D, \tag{1}$$

where

$$\begin{aligned}\widehat{H}_{cs} &= \hbar\sum_{j=1}^{N_s}\left(\omega_j - \overline{\omega}\right)\widehat{I}_{Z,j},\\ \widehat{H}_{\text{offset}} &= \hbar\Delta\omega\widehat{I}_Z\end{aligned} \tag{2}$$

are the chemical shift and resonance offset interactions, respectively, with $\overline{\omega} = \frac{1}{N}\sum_{j=1}^{N}\omega_j$ and $\Delta\omega = \overline{\omega} - \omega_{tr}$. In Eq. (2), $\widehat{I}_Z = \sum_{j=1}^{N_s}\widehat{I}_{Z,j}$, with $\widehat{I}_{Z,j}$, $\widehat{I}_{X,j}$, and $\widehat{I}_{Y,j}$ being the spin operators for spin j.

Under high-field conditions, the dipolar Hamiltonian, $\widehat{H}_D$, is given by

$$\frac{\widehat{H}_D}{\hbar} = \sum_{j<k}\omega_{D,jk}\left(3\widehat{I}_{Z,k}\widehat{I}_{Z,j} - \vec{\widehat{I}}_k\cdot\vec{\widehat{I}}_j\right), \tag{3}$$

where $\omega_{D,jk} = \frac{\gamma^2\hbar}{2r_{jk}^3}\left(1 - 3\cos^2(\theta_{jk})\right)$ is the dipolar coupling constant between spins j and k, with θ_{jk} being the angle that the internuclear vector, $\vec{r}_{jk} = \vec{r}_j - \vec{r}_k$, makes with respect to the $\widehat{z}$-axis.

Consider application of an RF pulse of amplitude $\omega_{RF}(t)$ applied along the $\widehat{y}$-direction in the rotating frame for a time T_p. The Hamiltonian during the pulse is given by $\widehat{H}(t) = \widehat{H}_0 + \widehat{H}_{RF}(t)$ for $0 \le t \le T_p$ with $\widehat{H}_{RF}(t) = \hbar\omega_{RF}(t)\widehat{I}_Y$. Starting with initial equilibrium $\widehat{z}$-magnetization, $\widehat{\rho}(0) = \widehat{\rho}_{eq} = \widehat{I}_Z$, the density matrix after application of an RF pulse in the LR regime is given by[14]

$$\begin{aligned}\widehat{\rho}_{LR}(T_p) &= \widehat{U}_{LR}(T_p)\widehat{\rho}_{eq}\widehat{U}_{LR}^{\dagger}(T_p)\\ &= \widehat{I}_Z - i\widehat{U}_0\left(T_p\right)\left(\int_0^{T_p}dt'\widehat{U}_0^{\dagger}(t')\left[\widehat{H}_{RF}(t'),\widehat{I}_Z\right]\widehat{U}_0(t')\right)\\ &\quad\times\widehat{U}_0^{\dagger}\left(T_p\right)\\ &= \widehat{I}_Z - i\widehat{U}_0\left(T_p\right)\left(\int_0^{T_p}dt'\omega_{RF}(t')\left[\widehat{U}_0^{\dagger}(t')\widehat{I}_Y\widehat{U}_0(t'),\widehat{I}_Z\right]\right)\\ &\quad\times\widehat{U}_0^{\dagger}\left(T_p\right)\\ &= \widehat{I}_Z - \frac{iT_p}{\hbar}\widehat{U}_0\left(T_p\right)\left[\overline{H}_{\text{AVG}}^{(1)}(T_p),\,\widehat{I}_Z\right]\widehat{U}_0^{\dagger}\left(T_p\right),\end{aligned} \tag{4}$$

where

$$\widehat{U}_{LR}(T_p) = \widehat{U}_0(T_p)\left(\widehat{1} - i\frac{T_p\overline{H}_{\text{AVG}}^{(1)}(T_p)}{\hbar}\right) \tag{5}$$

is the LR propagator, $\widehat{U}_0(t) = \exp\left(-i\frac{\widehat{H}_0 t}{\hbar}\right)$ is the propagator under free evolution, and $\overline{H}_{\text{AVG}}^{(1)}(T_p)$ is the first-order average Hamiltonian[16] of $\widehat{H}_{RF}(t)$ over a time T_p in the interaction frame defined by $\widehat{H}_0$,

$$\begin{aligned}\frac{\overline{H}_{\text{AVG}}^{(1)}(T_p)}{\hbar} &= \frac{1}{\hbar T_p}\int_0^{T_p}dt\widehat{U}_0^{\dagger}(t)\widehat{H}_{RF}(t)\widehat{U}_0(t)\\ &= \frac{1}{T_p}\int_0^{T_p}\mathrm{d}t\omega_{RF}(t)\widehat{U}_0^{\dagger}(t)\widehat{I}_Y\widehat{U}_0(t).\end{aligned} \tag{6}$$

Since $\left[\widehat{H}_D + \widehat{H}_{cs},\,\widehat{I}_Z\right] = 0$, $\overline{H}_{\text{AVG}}^{(1)}(T_p)$ in Eq. (6) can be written in a simultaneous eigenbasis of both $\widehat{H}_D + \widehat{H}_{cs}$ and $\widehat{I}_Z$, $\{|\varepsilon_{k,m},f\rangle\}$, with

$$\begin{aligned}\left(\widehat{H}_D + \widehat{H}_{cs}\right)|\varepsilon_{k,m},f\rangle &= \varepsilon_{k,m}|\varepsilon_{k,m},f\rangle,\\ \widehat{I}_Z|\varepsilon_{k,m},f\rangle &= m|\varepsilon_{k,m},f\rangle,\\ \langle\varepsilon_{k,m},f|\varepsilon_{p,n},g\rangle &= \delta_{kp}\delta_{mn}\delta_{fg},\end{aligned} \tag{7}$$

where the indices $g \neq f$ in Eq. (7) denote different, orthogonal states with identical eigenvalues of $\left(\widehat{H}_D + \widehat{H}_{cs}\right)$ and $\widehat{I}_Z$.

Using the eigenbasis in Eq. (7), $\overline{H}^{(1)}_{\text{AVG}}(T_p)$ can be written as

$$
\begin{aligned}
\frac{\overline{H}^{(1)}_{\text{AVG}}(T_p)}{\hbar} &= \frac{1}{T_p}\int_0^{T_p} \mathrm{d}t\omega_{RF}(t)\widehat{U}_0^{\dagger}(t)\widehat{I}_Y\widehat{U}_0(t) \\
&= \frac{1}{2iT_p}\int_0^{T_p} \mathrm{d}t\omega_{RF}(t)\widehat{U}_0^{\dagger}(t)\left[\widehat{I}_+ - \widehat{I}_-\right]\widehat{U}_0(t) \\
&= \frac{1}{2iT_p}\int_0^{T_p} \mathrm{d}t\omega_{RF}(t)\sum_{|\varepsilon_{k,m},d\rangle}\sum_{|\varepsilon_{j,m-1},f\rangle} e^{i\left(\omega_{k,j}^{m,m-1}+\Delta\omega\right)t} \\
&\quad \times \left[\widehat{I}_+\right]^{\varepsilon_{k,m},d}_{\varepsilon_{j,m-1},f}|\varepsilon_{k,m},d\rangle\langle\varepsilon_{j,m-1},f| + h.c.t.,
\end{aligned}
\tag{8}
$$

where $\left[\widehat{I}_\pm\right]^{\alpha}_{\beta} = \langle\alpha|\widehat{I}_\pm|\beta\rangle = \left(\left[\widehat{I}_\mp\right]^{\beta}_{\alpha}\right)^*$, $\omega_{k,j}^{a,b} = \frac{\varepsilon_{k,a}-\varepsilon_{j,b}}{\hbar}$, and "*h.c.t.*" denotes the Hermitian conjugate transpose (e.g., $\widehat{A} = a\widehat{B} + a^*\widehat{B}^{\dagger} \equiv a\widehat{B} + h.c.t.$).

For a constant RF pulse shape, $\omega_{RF}(t) = \omega_{RF}$ for $0 \le t \le T_p$, $\overline{H}^{(1)}_{\text{AVG}}(T_p)$ in Eq. (8) is given by

$$
\begin{aligned}
\frac{\overline{H}^{(1)}_{\text{AVG}}(T_p)}{\hbar} &= \frac{\omega_{RF}}{2i}\sum_{|\varepsilon_{k,m},d\rangle}\sum_{|\varepsilon_{j,m-1},f\rangle}\operatorname{sinc}\left(\frac{\left(\omega_{k,j}^{m,m-1}+\Delta\omega\right)T_p}{2}\right) \\
&\quad \times e^{i\frac{\left(\omega_{k,j}^{m,m-1}+\Delta\omega\right)T_p}{2}}\left[\widehat{I}_+\right]^{\varepsilon_{k,m},d}_{\varepsilon_{j,m-1},f}|\varepsilon_{k,m},d\rangle\langle\varepsilon_{j,m-1},f| \\
&\quad + h.c.t. \\
&= \frac{\omega_{RF}}{2i}\sum_{|\varepsilon_{k,m},d\rangle}\sum_{|\varepsilon_{j,m-1},f\rangle}\operatorname{sinc}\left(\frac{\left(\omega_{k,j}^{m,m-1}+\Delta\omega\right)T_p}{2}\right) \\
&\quad \times \left[\widehat{I}_+\right]^{\varepsilon_{k,m},d}_{\varepsilon_{j,m-1},f}\widehat{U}_0^{\dagger}\left(\frac{T_p}{2}\right)|\varepsilon_{k,m},d\rangle\langle\varepsilon_{j,m-1},f|\widehat{U}_0\left(\frac{T_p}{2}\right) \\
&\quad + h.c.t. \\
&= \widehat{U}_0^{\dagger}\left(\frac{T_p}{2}\right)\frac{\overline{\overline{H}}^{(1)}_{\text{AVG}}(T_p)}{\hbar}\widehat{U}_0\left(\frac{T_p}{2}\right).
\end{aligned}
\tag{9}
$$

Therefore, $\widehat{\rho}_{LR}(T_p)$ in Eq. (4) can be written for a constant RF pulse shape as

$$
\begin{aligned}
\widehat{\rho}_{LR}(T_p) &= \widehat{I}_Z - \frac{iT_p}{\hbar}\widehat{U}_0\left(T_p\right)\left[\overline{H}^{(1)}_{\text{AVG}}(T_p), \widehat{I}_Z\right]\widehat{U}_0^{\dagger}\left(T_p\right) \\
&= \frac{\widehat{I}_Z}{2} + \frac{\Theta}{2}\sum_{|\varepsilon_{k,m},d\rangle}\sum_{|\varepsilon_{j,m-1},f\rangle}\operatorname{sinc}\left(\frac{\left(\omega_{k,j}^{m,m-1}+\Delta\omega\right)T_p}{2}\right) \\
&\quad \times \left[\widehat{I}_+\right]^{\varepsilon_{k,m},d}_{\varepsilon_{j,m-1},f}\widehat{U}_0\left(\frac{T_p}{2}\right)|\varepsilon_{k,m},d\rangle \\
&\quad \times \langle\varepsilon_{j,m-1},f|\widehat{U}_0^{\dagger}\left(\frac{T_p}{2}\right) + h.c.t.,
\end{aligned}
\tag{10}
$$

where $\Theta = \int_0^{T_p}\mathrm{d}t'\omega_{RF}(t') = 2\pi\nu_{RF}T_p$ is the "nominal" flip-angle for a constant RF pulse shape.

The average free induction decay (FID) after application of a low-power pulse (LPP) in the LR regime is given by

$$
\begin{aligned}
\text{FID}^{LR}_{LPP}(t) &= \left\langle\!\!\left\langle\frac{\text{Trace}\left[\widehat{I}_+\widehat{U}_0(t)\widehat{\rho}_{LR}(T_p)\widehat{U}_0^{\dagger}(t)\right]}{\text{Trace}\left[\widehat{I}_+\widehat{I}_-\right]}\right\rangle\!\!\right\rangle \\
&= \frac{\Theta}{2^{N_s}N_s}\left\langle\!\!\left\langle\sum_{|\varepsilon_{k,m},d\rangle}\sum_{|\varepsilon_{j,m-1},f\rangle}\operatorname{sinc}\left(\frac{\left(\omega_{k,j}^{m,m-1}+\Delta\omega\right)T_p}{2}\right)\right.\right. \\
&\quad \left.\left.\times\left|\left[\widehat{I}_+\right]^{\varepsilon_{k,m},d}_{\varepsilon_{j,m-1},f}\right|^2 e^{i\left(\omega_{k,j}^{m,m-1}+\Delta\omega\right)\left(t+\frac{T_p}{2}\right)}\right\rangle\!\!\right\rangle \\
&= \left[\omega_{RF} * \text{FID}_{\frac{\pi}{2}Y}\right](t+T_p).
\end{aligned}
\tag{11}
$$

$\text{FID}^{LR}_{LPP}(t)$ in Eq. (11) represents the convolution[14] of a constant RF pulse shape with the FID from a hard $\left(\frac{\pi}{2}\right)_Y$-pulse acquire experiment,

$$
\begin{aligned}
\text{FID}_{\frac{\pi}{2}}(t) &= \left\langle\!\!\left\langle\frac{\text{Trace}\left[\widehat{I}_+\widehat{U}_0(t)\widehat{I}_X\widehat{U}_0^{\dagger}(t)\right]}{\text{Trace}\left[\widehat{I}_+\widehat{I}_-\right]}\right\rangle\!\!\right\rangle \\
&= \frac{1}{2^{N_s}N_s}\left\langle\!\!\left\langle\sum_{|\varepsilon_{k,m},d\rangle}\sum_{|\varepsilon_{j,m-1},f\rangle}\left|\left[\widehat{I}_+\right]^{\varepsilon_{k,m},d}_{\varepsilon_{j,m-1},f}\right|^2 e^{i\left(\omega_{k,j}^{m,m-1}+\Delta\omega\right)t}\right\rangle\!\!\right\rangle,
\end{aligned}
\tag{12}
$$

where $\langle\langle\ \rangle\rangle$ indicates that an average over offsets, $\Delta\omega$ (say, due to ABMS, CSA, B_0 inhomogeneity, etc.), and crystallite orientations defined by the Euler angles $\Omega = (\alpha, \beta, \gamma)$ is being performed. For an observable $\widehat{A}$, $\langle\langle\widehat{A}\rangle\rangle \equiv \int\mathrm{d}\Omega\int\mathrm{d}(\Delta\omega)p_{\text{orientational}}(\Omega)p_{\text{offset}}(\Delta\omega)A(\Omega,\Delta\omega)$, where $p_{\text{orientational}}(\Omega)p_{\text{offset}}(\Delta\omega)$ is the joint probability density distribution for Ω and $\Delta\omega$. In polycrystalline or powdered samples, performing an orientational average is necessary due to the implicit Ω-dependence of the energies and eigenstates in Eq. (7).

No spectral diffusion under RF excitation is observed in the LR results in Eq. (11) since the contributions to $\text{FID}^{LR}_{LPP}(t)$ arise from transitions with the same transition frequency, $\left(\omega_{k,j}^{m,m-1}\right)$, both *during* the RF pulse (associated with time T_p) and *after* the RF pulse during the free evolution period (associated with time t). Accounting for the effects of spectral diffusion on FID_{LPP} therefore requires going beyond LR theory to at least third-order in the applied RF. It should be noted that the results in Eq. (12) are reminiscent of the LR result for inhomogeneously broadened spin systems.[14] One consequence is that the behavior of both inhomogeneously and homogeneously broadened spin systems under low-power excitation is predicted to be similar in the LR regime, which is consistent with previous experimental observations.[10]

The LR response result in Eq. (11) is therefore expected to be a good approximation to the dynamics when both the following conditions are satisfied: (**A**) for excitations in the LR regime ($\Theta \le \frac{\pi}{3}$) and (**B**) for transitions where the RF represents a weak perturbation, i.e., $|\omega_{k,j}^{m,m-1} + \Delta\omega| \gg \omega_{RF}$. However, for transitions where the RF represents a strong perturbation, $|\omega_{k,j}^{m,m-1} + \Delta\omega| \le \omega_{RF}$, LR theory can break down.[14] In particular, the transition from a weak to a strong perturbation can lead to errors in the LR predicted spectrum[14] near frequencies $|\nu| \le \omega_{RF}$, even in the LR regime ($\Theta \le \frac{\pi}{3}$).

It was previously demonstrated[14] that the LR results can be improved by using a unitarity-corrected LR propagator

$$\begin{aligned}\widehat{U}_{LR}^{\text{corr.}}(T_p,0) &= \widehat{U}_0(T_p)\left[\widehat{1}+\left(\frac{\overline{H}^{(1)}_{AVG}(T_p)T_p}{\hbar}\right)^2\right]^{-\frac{1}{2}}\\ &\quad\times\widehat{U}_0^{\dagger}(T_p)\widehat{U}_0(T_p)\left(\widehat{1}-i\frac{\overline{H}^{(1)}_{AVG}(T_p)T_p}{\hbar}\right)\\ &= \widehat{U}_0\left(\frac{T_p}{2}\right)\widetilde{V}\widehat{U}_0^{\dagger}\left(\frac{T_p}{2}\right)\widehat{U}_{LR}(T_p), \end{aligned}\tag{13}$$

where

$$\begin{aligned}\widetilde{V} &= \left(\widehat{1}+\left(\frac{T_p\overline{\overline{H}}^{(1)}_{\text{AVG}}(T_p)}{\hbar}\right)^2\right)^{-\frac{1}{2}}\\ &\approx \widehat{1}-\frac{1}{2}\left(\frac{T_p\overline{\overline{H}}^{(1)}_{\text{AVG}}(T_p)}{\hbar}\right)^2+\frac{3}{8}\left(\frac{T_p\overline{\overline{H}}^{(1)}_{\text{AVG}}(T_p)}{\hbar}\right)^4+\ldots.\end{aligned}\tag{14}$$

In effect, $\widetilde{V}$ acts like a "time-dependent" normalization[17] of the first-order eigenstates of the perturbed Hamiltonian, thereby ensuring that $\widehat{U}_{LR}^{\text{corr.}}(T_p,0)$ is unitary,

$$\left(\widehat{U}_{LR}^{\text{corr.}}(T_p,0)\right)^{\dagger}\widehat{U}_{LR}^{\text{corr.}}(T_p,0)=\widehat{U}_{LR}^{\text{corr.}}(T_p,0)\left(\widehat{U}_{LR}^{\text{corr.}}(T_p,0)\right)^{\dagger}=\widehat{1}. \tag{15}$$

For an inhomogeneously broadened system of spin-$\frac{1}{2}$ particles ($\widehat{H}_0=\hbar\omega\widehat{I}_Z$), $\widetilde{V}$ has a simple form[14] given by

$$\begin{aligned}\widetilde{V} &= v(\omega)\widehat{1},\\ v(\omega) &= \left(1+\left|\int_0^{T_p}\frac{\omega_{RF}(t')e^{i\omega t'}}{2}\right|^2\right)^{-\frac{1}{2}}\le 1,\end{aligned}\tag{16}$$

where $\widehat{1}$ is the 2×2 identity matrix, ω is the transition frequency, and $v(\omega)$ is a frequency dependent renormalization factor. For $\Theta\le\frac{\pi}{3}$, $v(\omega)\to 1$ for $|\omega T_p|\gg|\Theta|$, whereas $v(\omega)\to\left(1+\frac{\Theta^2}{4}\right)^{-1/2}<1$ for $|\omega T_p|\ll|\Theta|$.

In dipolar systems, $\widetilde{V}$ will possess non-zero off-diagonal elements due to the interconnectedness of the eigenstates of $\widehat{H}_D$ under RF excitation. However, the diagonal elements of $\widetilde{V}$ are less than 1, $\left[\widetilde{V}\right]^{\varepsilon_{k,m},d}_{\varepsilon_{k,m},d}\le 1$, as demonstrated in Appendix B and have a similar effect like $v(\omega)$ for the spin-1/2 case in Eq. (16). For those states $|\varepsilon_{k,m},d\rangle$ that are only weakly coupled to all other states $|\varepsilon_{j,m\pm1},f\rangle$ via $\overline{H}_{\text{AVG}}(T_p)$ in Eq. (9), i.e., $|\omega^{m,m-1}_{k,j}+\Delta\omega|\gg\omega_{RF}$, $\left[\widetilde{V}\right]^{\varepsilon_{k,m},d}_{\varepsilon_{k,m},d}\approx 1$. By enforcing unitarity of $\widehat{U}_{LR}^{\text{corr.}}$ in Eq. (13), spectral diffusion during the RF pulse, which is represented by the off-diagonal elements of $\widetilde{V}$, has been "artificially" introduced in the LR results without directly performing third- and higher-order calculations in ω_{RF}.

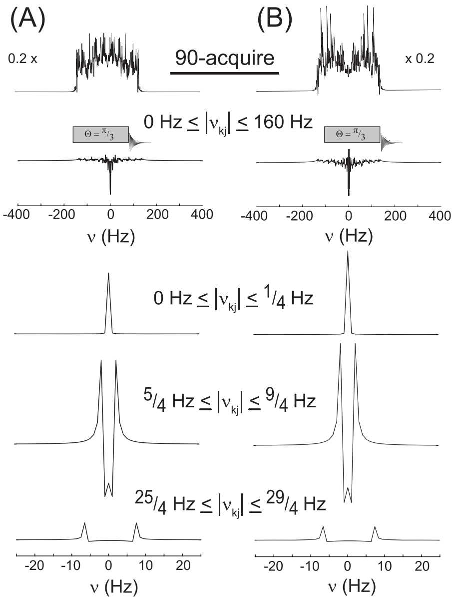

FIG. 1. Numerical simulations (Δt = 1 ms, N_{pts} = 1000) of the spectra after low-power excitation by a constant RF pulse (ν_{RF} = 1 Hz and $\Theta=\frac{\pi}{3}$) in an N_s = 10 linear ($I=\frac{1}{2}$) spin chain with a spin configuration, $\vec{r}_{\text{spins}}$, given either by (a) $\vec{r}_{\text{spins}_1}$ = [0.0152, 1.0587, 2.0986, 2.9865, 3.9334, 4.9609, 5.9602, 7.0007, 7.9560, 8.9561]$d\widehat{z}$ or by (b) $\vec{r}_{\text{spins}_2}$ = [0.0509, 0.9746, 2.0785, 3.0807, 3.9546, 4.9244, 6.0782, 7.0395, 8.0684, 8.9516]$d\widehat{z}$, where d is the average spacing between nearest spins with $\frac{\gamma^2\hbar}{2\pi d^3}$ = 35 Hz. The corresponding $\frac{\pi}{2}$-acquire spectra are given at the top. For both $\vec{r}_{\text{spins}_1}$ and $\vec{r}_{\text{spins}_2}$, most single-quantum transitions, $\nu^{m,m-1}_{k,j}$ were within the range $\left|\nu^{m,m-1}_{k,j}\right|\le$ 160 Hz. After low-power excitation, negative spectral intensity near $\nu\approx$ 0 Hz was observed for both $\vec{r}_{\text{spins}_1}$ and $\vec{r}_{\text{spins}_2}$ although the magnitude of the spectral intensity near $\nu\approx$ 0 Hz was twice as large for $\vec{r}_{\text{spins}_1}$ relative to $\vec{r}_{\text{spins}_2}$. This negative spectral intensity was a result of destructive interference from transitions with $|\nu^{m,m-1}_{k,j}|>$ 0 Hz which can be seen by comparing the exact contributions to the spectrum from transitions in the range 0 Hz $\le\left|\nu^{m,m-1}_{k,j}\right|\le\frac{1}{4}$ Hz (positive for both $\vec{r}_{\text{spins}_1}$ and $\vec{r}_{\text{spins}_2}$), from transitions in the range $\frac{5}{4}$ Hz $\le\left|\nu^{m,m-1}_{k,j}\right|\le\frac{9}{4}$ Hz (symmetrical and dispersive about ν = 0 Hz with negative intensity at ν = 0 Hz), and from transitions in the range $\frac{25}{4}$ Hz $\le\left|\nu^{m,m-1}_{k,j}\right|\le\frac{29}{4}$ Hz (slightly dispersive with negative intensity at ν = 0 Hz).

In this case, the density matrix using $\widehat{U}_{LR}^{\text{corr.}}(T_p,0)$ is given by

$$\begin{aligned}\widehat{\rho}_{LR}^{\text{corr.}}(T_p) &= \widehat{U}_{LR}^{\text{corr.}}(T_p,0)\widehat{I}_Z\left(\widehat{U}_{LR}^{\text{corr.}}(T_p,0)\right)^{\dagger}\\ &= \widehat{U}_0\left(\frac{T_p}{2}\right)\widetilde{V}\widehat{U}_0^{\dagger}\left(\frac{T_p}{2}\right)\left(\widehat{\rho}_{LR}(T_p)+\widehat{U}_0(T_p)\frac{T_p\overline{H}^{(1)}_{\text{AVG}}(T_p)}{\hbar}\widehat{I}_Z\frac{T_p\overline{H}^{(1)}_{\text{AVG}}(T_p)}{\hbar}\widehat{U}_0^{\dagger}(T_p)\right)\widehat{U}_0\left(\frac{T_p}{2}\right)\widetilde{V}^{\dagger}\widehat{U}_0^{\dagger}\left(\frac{T_p}{2}\right),\end{aligned}\tag{17}$$

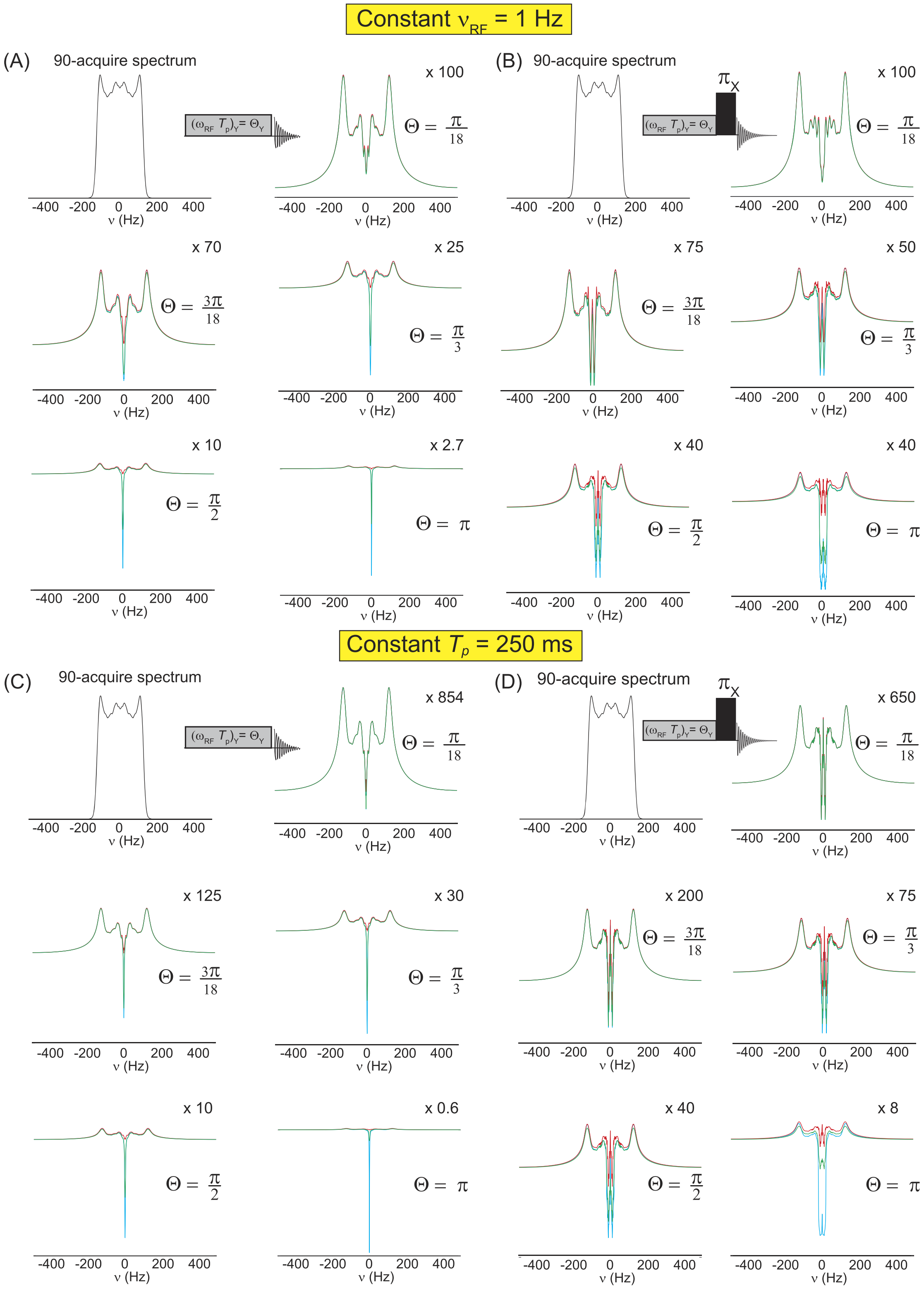

FIG. 2. Numerical simulation of the spectra under $\widehat{H}_0 = \widehat{H}_D + \hbar\Delta\omega\widehat{I}_Z$ derived from low-power excitation by a constant RF pulse shape, with and without application of a π_X-pulse, in an $N_s = 10$ linear spin chain averaged over 200 different spatial configurations. For each $\vec{r}_{\text{spins}}$, the evolution for 41 different values of $\Delta\omega$ uniformly distributed over the range $\frac{\Delta\omega}{2\pi} \in [-10\,\text{Hz},\ 10\,\text{Hz}]$ was averaged for $\Theta = 2\pi\nu_{RF}T_p \in \left\{\frac{\pi}{18}, \frac{\pi}{6}, \frac{\pi}{3}, \frac{\pi}{2}, \pi\right\}$ under conditions of either constant ν_{RF} [$\nu_{RF} = 1$ Hz in Figs. 2(a) and 2(b)] or constant T_p [$T_p = 250$ ms in Figs. 2(c) and 2(d)]. The (blue) exact spectra along with those calculated using [Eq. (11), red] LR and [Eq. (17), green] unitarity-corrected LR theory are shown. The (blue) exact spectra after low-power excitation for both fixed (a) ν_{RF} and (c) T_p contained a negative "dip" near the RF transmitter frequency [$|\nu| \approx 0$ Hz] that became more pronounced with increasing Θ. The spectra from low-power excitation followed by a π_X-pulse became more negative with increasing Θ near $|\nu| \approx 0$ Hz for both fixed (b) ν_{RF} and (d) T_p, although a "peak" was generated at $\nu \approx 0$ Hz. For $\Theta = \frac{\pi}{18}$, both the (red) LR and (green) unitarity-corrected LR spectra matched the (blue) exact spectra. For $\Theta \geq \frac{\pi}{6}$, the unitarity-corrected LR spectra showed a similar trend to the exact spectra with increasing Θ while the LR spectra remained relatively unchanged. In all simulations, $N_{pts} = 1000$ and $\Delta t = 1$ ms.

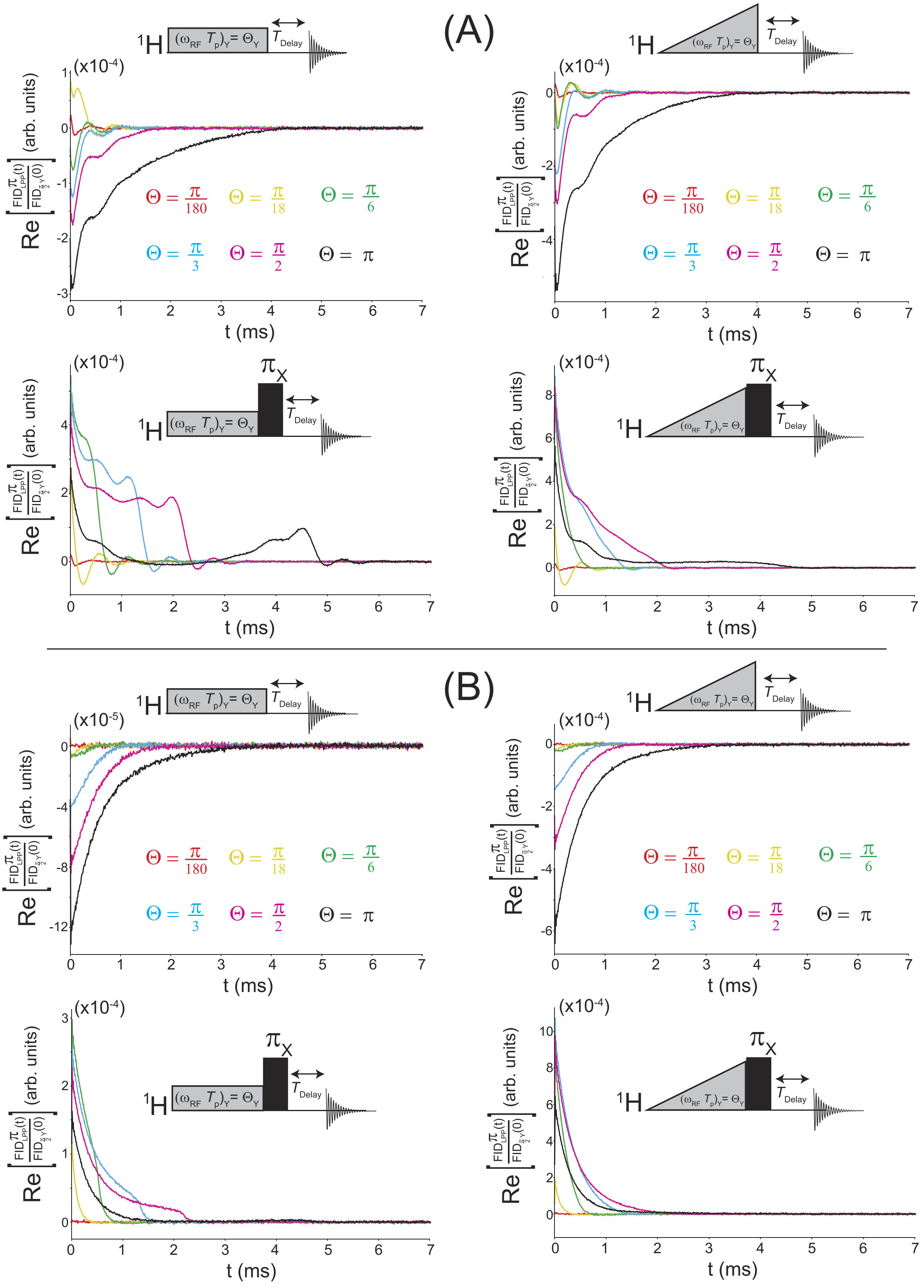

FIG. 3. Experimental FID$_{LLP}(t)$ and FID$^{\pi}_{LLP}(t)$ for fixed $\frac{\omega_{RF}}{2\pi} = \nu_{RF} = 100$ Hz in powdered (a) adamantane and (b) ferrocene using either a constant (left, $\frac{\omega_{RF}(t)}{2\pi} = \nu_{RF}$ for $0 \le t \le T_p$) or a ramped (right, $\frac{\omega_{RF}(t)}{2\pi} = \frac{2\nu_{RF}}{T_p}t$ for $0 \le t \le T_p$) pulse shape for different "nominal" flip-angles $\Theta \in \left\{\frac{\pi}{180}, \frac{\pi}{18}, \frac{\pi}{6}, \frac{\pi}{3}, \frac{\pi}{2}, \pi\right\}$. All FIDs, which are plotted with an acquisition delay of $T_{\text{Delay}} = 150\ \mu$s placed after the last RF pulse, are normalized by the first point of the corresponding FID$_{\frac{\pi}{2}Y}(0)$.

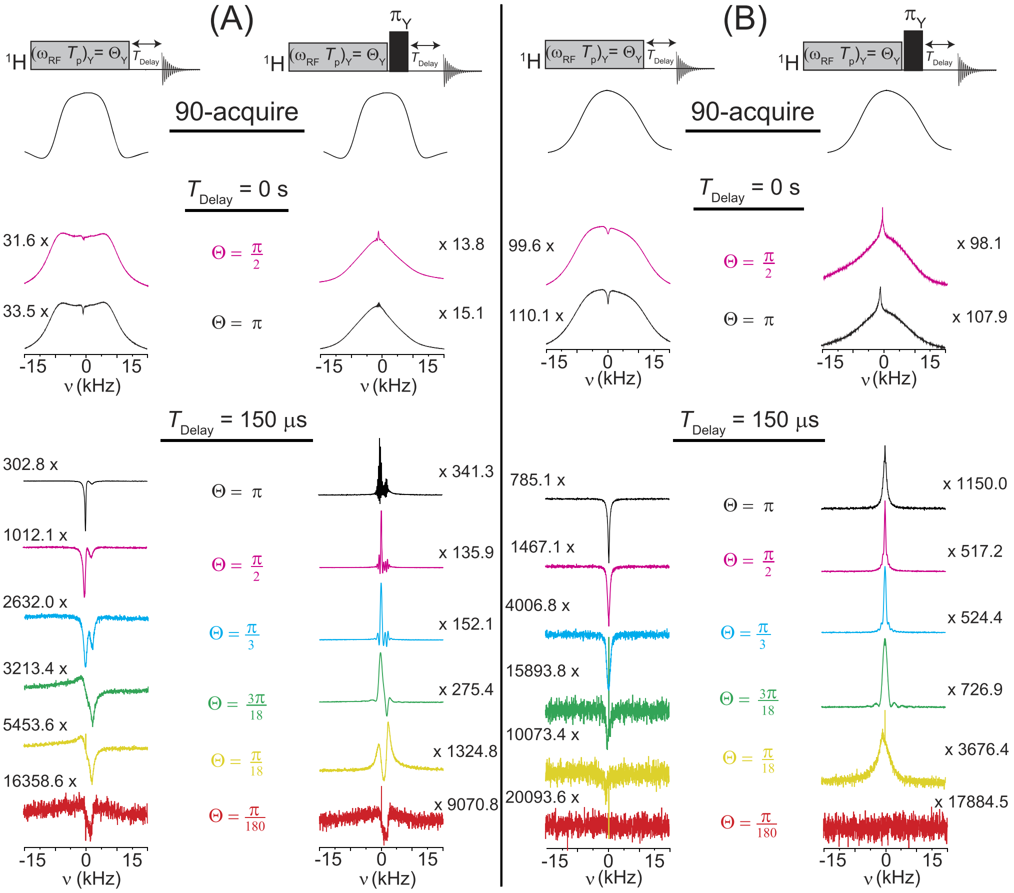

FIG. 4. Experimental spectra of powdered (a) adamantane and (b) ferrocene derived from Fourier transformation of the various $\mathrm{FID}_{LPP}(t)$ and $\mathrm{FID}^{\pi}_{LPP}(t)$ in Fig. 3 using a constant pulse shape. Compared with the corresponding $\frac{\pi}{2}$-acquire spectra in adamantane and ferrocene (shown at the top), the spectra obtained after low-power excitation (with $T_{\mathrm{Delay}} = 0$ s and $\Theta = \frac{\pi}{2}$ and $\Theta = \pi$) were broader with a small "dip" near $\nu \approx 0$ Hz, whereas the corresponding spectra derived from $\mathrm{FID}^{\pi}_{LPP}(t)$ were narrower with a "peak" near $\nu \approx 0$ Hz. With an acquisition delay of $T_{\mathrm{Delay}} = 150\ \mu$s, only a "dip" or "peak" remained that increased in intensity as Θ increased. (a) In adamantane, interference between the additional resonance at $\nu \approx 1.74$ kHz and the "dip"/"peak" near $\nu \approx 0$ Hz was observed for $\Theta < \frac{\pi}{3}$. Scaling factors with respect to the $\frac{\pi}{2}$-acquire spectra are shown next to each spectrum.

with the corresponding unitarity-corrected FID in the LR regime given by

$$
\begin{aligned}
\mathrm{FID}^{LR\,\mathrm{corr.}}_{LPP}(t) &= \left\langle\!\!\left\langle \frac{\mathrm{Trace}\left[\widehat{I}_+\widehat{U}_0\left(t+\frac{T_p}{2}\right)\widetilde{V}\widehat{U}_0^{\dagger}\left(\frac{T_p}{2}\right)\widehat{\rho}_{LR}(T_p)\widehat{U}_0\left(\frac{T_p}{2}\right)\widetilde{V}^{\dagger}\widehat{U}_0^{\dagger}\left(t+\frac{T_p}{2}\right)\right]}{\mathrm{Trace}\left[\widehat{I}_+\widehat{I}_-\right]}\right\rangle\!\!\right\rangle \\
&= \frac{\Theta}{2^{N_s}N_s}\left\langle\!\!\left\langle \sum_{|\varepsilon_{k,m},d\rangle}\sum_{|\varepsilon_{j,m-1,f}\rangle}\sum_{|\varepsilon_{l,m+n,c}\rangle}\sum_{|\varepsilon_{p,m+n-1,b}\rangle}\left[\widehat{I}_+\right]^{\varepsilon_{k,m},d}_{\varepsilon_{j,m-1},f}\left[\widehat{I}_-\right]^{\varepsilon_{p,m+n-1},b}_{\varepsilon_{l,m+n},c}\right.\right. \\
&\quad \left.\left.\times\left[\widetilde{V}\right]^{\varepsilon_{j,m-1},f}_{\varepsilon_{p,m+n-1},b}\left[\widetilde{V}\right]^{\varepsilon_{k,m},d}_{\varepsilon_{l,m+n},c}\mathrm{sinc}\left(\frac{\left(\omega^{m+n,m+n-1}_{l,p}+\Delta\omega\right)}{2}T_p\right)e^{i\left(\omega^{m,m-1}_{k,j}+\Delta\omega\right)\left(t+\frac{T_p}{2}\right)}\right\rangle\!\!\right\rangle. \qquad (18)
\end{aligned}
$$

In Eq. (18), spectral diffusion during the pulse can occur between transitions with frequencies $\omega^{m+n,m+n-1}_{l,p} \neq \omega^{m,m-1}_{k,j}$ for $n = \{0, \pm 2, \pm 4, \cdots\}$. This can be more clearly seen by expanding Eq. (18) as

$$
\begin{aligned}
\mathrm{FID}^{LR\,\mathrm{corr.}}_{LPP}(t) &= \frac{\Theta}{2^{N_s}N_s}\left\langle\!\!\left\langle \sum_{|\varepsilon_{k,m},d\rangle}\sum_{|\varepsilon_{j,m-1,f}\rangle}\left|\left[\widehat{I}_+\right]^{\varepsilon_{k,m},d}_{\varepsilon_{j,m-1},f}\right|^2\left[\widetilde{V}\right]^{\varepsilon_{j,m-1},f}_{\varepsilon_{j,m-1},f}\left[\widetilde{V}\right]^{\varepsilon_{k,m},d}_{\varepsilon_{k,m},d}\mathrm{sinc}\left(\frac{\left(\omega^{m,m-1}_{k,j}+\Delta\omega\right)}{2}T_p\right)e^{i\left(\omega^{m,m-1}_{k,j}+\Delta\omega\right)\left(t+\frac{T_p}{2}\right)}\right\rangle\!\!\right\rangle \\
&\quad + \frac{\Theta}{2^{N_s}N_s}\left\langle\!\!\left\langle \sum_{|\varepsilon_{k,m},d\rangle}\sum_{|\varepsilon_{j,m-1,f}\rangle}\sum_{|\varepsilon_{l,m},c\rangle\neq|\varepsilon_{k,m},d\rangle}\sum_{|\varepsilon_{p,m-1,b}\rangle\neq|\varepsilon_{j,m-1},f\rangle}\left[\widehat{I}_+\right]^{\varepsilon_{k,m},d}_{\varepsilon_{j,m-1},f}\left[\widehat{I}_-\right]^{\varepsilon_{p,m-1},b}_{\varepsilon_{l,m},c}\left[\widetilde{V}\right]^{\varepsilon_{j,m-1},f}_{\varepsilon_{p,m-1},b}\left[\widetilde{V}\right]^{\varepsilon_{k,m},d}_{\varepsilon_{l,m},c}\mathrm{sinc}\left(\frac{\left(\omega^{m,m-1}_{l,p}+\Delta\omega\right)}{2}T_p\right)\right. \right.\\
&\quad \left.\left.\times\, e^{i\left(\omega^{m,m-1}_{k,j}+\Delta\omega\right)\left(t+\frac{T_p}{2}\right)}\right\rangle\!\!\right\rangle + \frac{\Theta}{2^{N_s}N_s}\sum_{n=\{\pm2,\pm4,\pm6,\ldots\}}\left\langle\!\!\left\langle \sum_{|\varepsilon_{k,m},d\rangle}\sum_{|\varepsilon_{j,m-1,f}\rangle}\sum_{|\varepsilon_{l,m+n},c}\sum_{|\varepsilon_{p,m-1+n},b\rangle}\left[\widehat{I}_+\right]^{\varepsilon_{k,m},d}_{\varepsilon_{j,m-1},f}\left[\widehat{I}_-\right]^{\varepsilon_{p,m-1+n},b}_{\varepsilon_{l,m+n},c}\right.\right. \\
&\quad \left.\left.\times\left[\widetilde{V}\right]^{\varepsilon_{j,m-1},f}_{\varepsilon_{p,m-1+n},b}\left[\widetilde{V}\right]^{\varepsilon_{k,m},d}_{\varepsilon_{l,m+n},c}\mathrm{sinc}\left(\frac{\left(\omega^{m+n,m-1+n}_{l,p}+\Delta\omega\right)}{2}T_p\right)e^{i\left(\omega^{m,m-1}_{k,j}+\Delta\omega\right)\left(t+\frac{T_p}{2}\right)}\right\rangle\!\!\right\rangle. \qquad (19)
\end{aligned}
$$

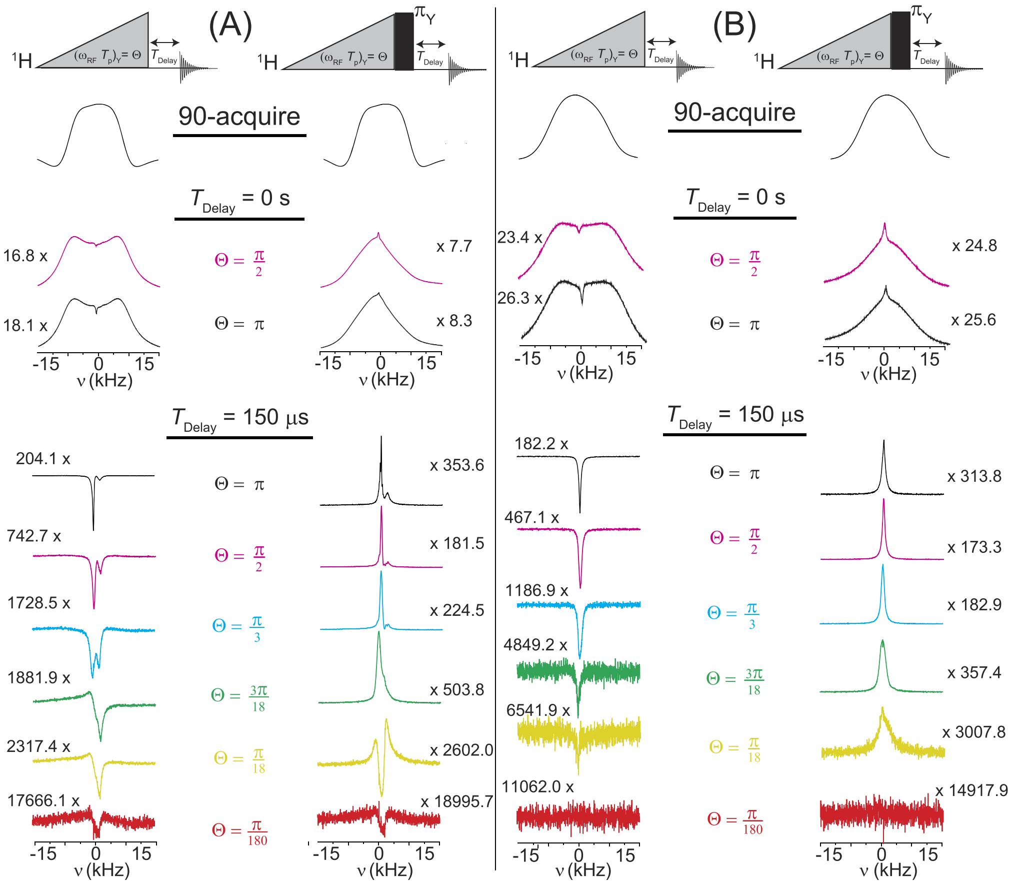

FIG. 5. Experimental spectra of powdered (a) adamantane and (b) ferrocene derived from Fourier transformation of the various FID$_{LPP}(t)$ and FID$^{\pi}_{LPP}(t)$ in Fig. 3 using a ramped pulse shape ($\frac{\omega_{RF}(t)}{2\pi} = \frac{2\nu_{RF}}{T_p}t$ for $0 \le t \le T_p$ and $\nu_{RF} = 100$ Hz). Compared with the corresponding $\frac{\pi}{2}$-acquire spectra in adamantane and ferrocene (shown at the top), the spectra obtained after low-power excitation (with $T_{\text{Delay}} = 0$ s and $\Theta = \frac{\pi}{2}$ and $\Theta = \pi$) were broader with a small "dip" near $\nu \approx 0$ Hz, whereas the corresponding spectra derived from FID$^{\pi}_{LPP}(t)$ were narrower with a small "peak" near $\nu \approx 0$ Hz. With an acquisition delay of $T_{\text{Delay}} = 150\ \mu$s, only the "dip" or "peak" remained that increased in intensity as Θ increased. (a) In adamantane, interference between the additional resonance at $\nu \approx 1.74$ kHz and the "dip"/"peak" near $\nu \approx 0$ Hz was observed for $\Theta < \frac{\pi}{3}$. Scaling factors with respect to the $\frac{\pi}{2}$-acquire spectra are shown next to each spectrum.

The first term in Eq. (19) represents the direct contribution to the FID from single-quantum transitions generated by low-power RF excitation *without* spectral diffusion, which is similar to the LR result in Eq. (11). The next two terms in Eq. (19) represent contributions to FID$^{LR,\text{corr.}}_{LPP}(t)$ from transitions that have undergone spectral diffusion during the pulse.

In Fig. 1, numerical simulations of an $N_s = 10$ linear spin $\left(I = \frac{1}{2}\right)$ chain are shown. The spin chain was arranged along the $\hat{z}$-axis, and an even number of spins were chosen in order to avoid accidental single-quantum degeneracies that exist due to the invariance of $\hat{H}_D$ under a π-pulse.[18] In the simulations, the position of the kth spin, $\vec{r}_k$, was randomly chosen to be within the interval $[(k-1.1)d\hat{z}, (k-0.9)d\hat{z}]$ for all $k \in \{1, 2, \ldots, 10\}$, where d is the average separation between nearest neighbors. In this case, the dipolar coupling constant between spins j and k was given by $\frac{\omega_{D,jk}}{2\pi} = -\frac{\gamma^2\hbar}{2\pi|\vec{r}_j-\vec{r}_k|^3} = -\frac{\gamma^2\hbar}{2\pi d^3}\frac{1}{\left|\frac{\vec{r}_j}{d}-\frac{\vec{r}_k}{d}\right|^3} = -\frac{35\text{ Hz}}{\left|\frac{\vec{r}_j}{d}-\frac{\vec{r}_k}{d}\right|^3}$. In Fig. 1, simulations are shown for two different spin arrangements, [Fig. 1(a)] $\vec{r}_{\text{spins}_1}$ and [Fig. 1(b)] $\vec{r}_{\text{spins}_2}$ (see the caption of Fig. 1 for more details). The exact FID under $\hat{H}_D = \frac{\hbar}{2}\sum_{j=1}^{10}\sum_{k\neq j}\omega_{D,jk}\left(2\hat{I}_{Z,j}\hat{I}_{Z,k} - \hat{I}_{X,j}\hat{I}_{X,k} - \hat{I}_{Y,j}\hat{I}_{Y,k}\right)$ after application of a constant RF pulse ($\nu_{RF} = 1$ Hz with $\Theta = \frac{\pi}{3}$) was numerically calculated at times $t = k\Delta t$ for $k = 0$ to $k = 999$ with $\Delta t = 1$ ms. For both spin configurations, the majority of single-quantum transitions were within the frequency range -160 Hz $\le \nu \le 160$ Hz, as seen from the $\frac{\pi}{2}$-acquire spectra given at the top of Fig. 1. In Fig. 1(a), low-power excitation generated a negative "dip" in spectral intensity for $|\nu| < 2$ Hz, whereas in Fig. 1(b), the negative "dip" was roughly 50% smaller in intensity and narrower ($|\nu| < 1.6$ Hz).

In order to get a qualitative understanding of the simulations in Fig. 1, the exact contributions to FID$_{LPP}(t)$ from different ranges of transition frequency, $\nu^{m,m-1}_{k,j}$, are plotted. For both $\vec{r}_{\text{spins}_1}$ and $\vec{r}_{\text{spins}_2}$, the contribution from transitions within the range $0\,\text{Hz} \le \left|\nu^{m,m-1}_{k,j}\right| \le \frac{1}{4}$ Hz was positive and larger for $\vec{r}_{\text{spins}_2}$ than for $\vec{r}_{\text{spins}_1}$. For transitions in the range $\frac{5}{4}\,\text{Hz} \le \left|\nu^{m,m-1}_{k,j}\right| \le \frac{9}{4}$ Hz, the spectra appeared symmetrical and dispersive about $\nu = 0$ Hz with negative spectral intensity near $|\nu| \approx 0$ Hz. For transitions in the range $\frac{25}{4}\,\text{Hz} \le \left|\nu^{m,m-1}_{k,j}\right| \le \frac{29}{4}$ Hz, the spectra were only slightly dispersive with small, but negative, spectral intensity near $|\nu| \approx 0$ Hz. Summing up the contributions for transition

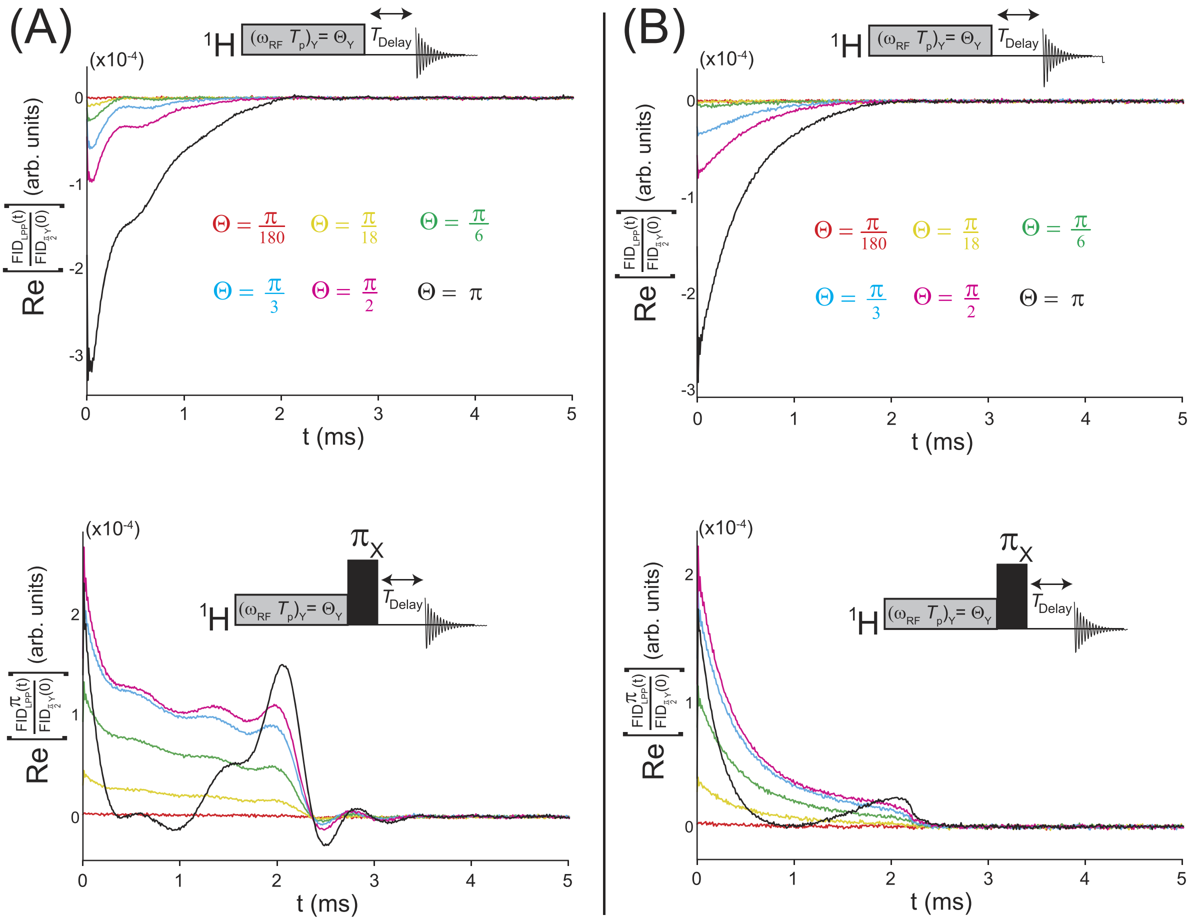

FIG. 6. Experimental $\mathrm{FID}_{LLP}(t)$ and $\mathrm{FID}^{\pi}_{LLP}(t)$ for a constant pulse shape of fixed length (T_p = 2.5 ms) in powdered (a) adamantane and (b) ferrocene for different "nominal" flip-angles $\Theta = 2\pi\nu_{RF}T_p \in \left\{\frac{\pi}{180}, \frac{\pi}{18}, \frac{\pi}{6}, \frac{\pi}{3}, \frac{\pi}{2}, \pi\right\}$. All FIDs, which are plotted with an acquisition delay of T_{Delay} = 150 μs placed after the last RF pulse, are normalized by the first point of the corresponding $\mathrm{FID}_{\frac{\pi}{2}Y}(0)$.

frequencies over the range $-160\,\mathrm{Hz} \le \nu^{m,m-1}_{k,j} \le 160$ Hz resulted in a negative "dip" near $\nu \approx 0$ Hz due to the interference of dispersive signals from $\left|\nu^{m,m-1}_{k,j}\right| > 0$ Hz. Such behavior was also observed for inhomogeneously broadened spin systems[14] and is similar to the Fung and Ermakov model[8] for selective excitation in dipolar systems. It should be noted that whether a negative "dip" was observed in the spin chain simulations depended upon $\vec{r}_{\mathrm{spin}}$ and, more generally, upon the distribution of transition frequencies, $\nu^{m,m-1}_{k,j}$, and their amplitudes, $\left|\left[\widehat{I}_+\right]^{\varepsilon_{k,m},d}_{\varepsilon_{j,m-1},f}\right|^2$. However, the spectral intensity near $\nu \approx 0$ Hz was always smaller (more negative) in the exact and the unitarity-corrected LR [Eq. (18)] calculations than those obtained using LR theory [Eq. (11)].

B. Application of a π_X-pulse after low-power excitation and the effect of nonzero $\widehat{H}_{cs}$

In the absence of chemical shift differences ($\widehat{H}_{cs} = 0$), application of a π_X-pulse after low-power excitation only affects the offset term of $\widehat{H}_0$ since $\widehat{R}_X(\pi)\widehat{I}_Z\widehat{R}^{\dagger}_X(\pi) = -\widehat{I}_Z$ while $\widehat{R}_X(\pi)\widehat{H}_D\widehat{R}^{\dagger}_X(\pi) = \widehat{H}_D$, where $\widehat{R}_X(\theta) = \exp\left(-i\theta\widehat{I}_X\right)$ represents a spin rotation of angle θ about the $\widehat{x}$-axis. In the absence of nonzero chemical shift differences, the states $|\varepsilon_{k,m}, d\rangle$ and $|\varepsilon_{k,-m}, d\rangle$ are degenerate and related to each other by $|\varepsilon_{k,m}, d\rangle \propto \widehat{R}_X(\pi)|\varepsilon_{k,-m}, d\rangle$. The unitarity-corrected LR FID under low-power excitation followed by a π_X-pulse, $\mathrm{FID}^{\pi,LR\,\mathrm{corr.}}_{LPP}(t)$, is given by

$$\mathrm{FID}^{\pi,LR\,\mathrm{corr.}}_{LPP}(t) = \frac{\Theta}{2^{N_s}N_s}\left\langle\!\!\left\langle \sum_{|\varepsilon_{k,m},d\rangle}\sum_{|\varepsilon_{j,m-1,f}\rangle}\sum_{|\varepsilon_{l,n-m,c}\rangle}\sum_{|\varepsilon_{p,n-m+1,b}\rangle}\left[\widehat{I}_+\right]^{\varepsilon_{k,m},d}_{\varepsilon_{j,m-1},f} \times \left[\widehat{I}_-\right]^{\varepsilon_{p,n-m+1},b}_{\varepsilon_{l,n-m},c}\left[\widetilde{V}\right]^{\varepsilon_{j,-m+1},f}_{\varepsilon_{p,n-m+1},b}\left[\widetilde{V}\right]^{\varepsilon_{k,-m},d}_{\varepsilon_{l,n-m},c} \times \mathrm{sinc}\left(\frac{\left(\omega^{n-m,n-m+1}_{l,p} + \Delta\omega\right)}{2}T_p\right)e^{i\omega^{m,m-1}_{k,j}\left(t+\frac{T_p}{2}\right)} \times e^{i\Delta\omega\left(t-\frac{T_p}{2}\right)}\right\rangle\!\!\right\rangle. \tag{20}$$

From Eq. (20), application of a π_X-pulse refocuses the inhomogeneous dephasing at time $t = \frac{T_p}{2}$ that occurred during the pulse from the distribution of $\Delta\omega$ that is due to the orientational dependence of ABMS and/or CSA in a powdered sample and/or B_0 inhomogeneity. At time $t = T_p$, the amount of inhomogeneous dephasing due to the distribution of $\Delta\omega$ is identical to the inhomogeneous dephasing prior to the π_X-pulse.

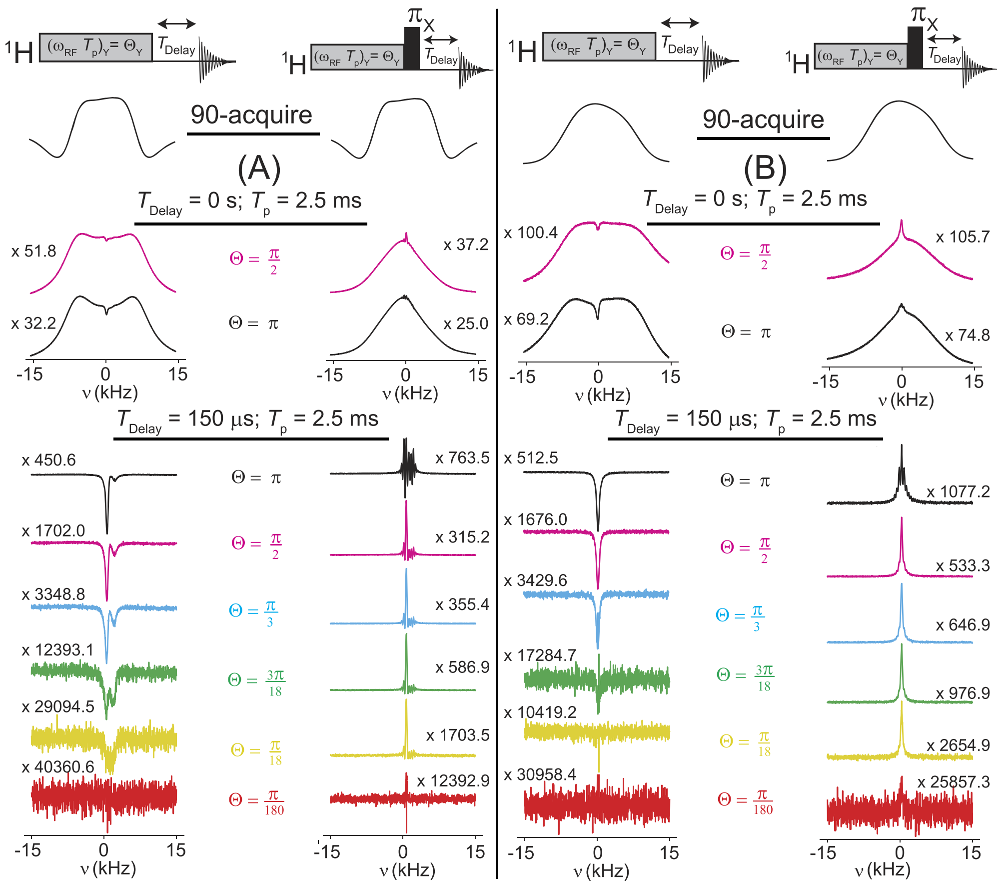

FIG. 7. Experimental spectra of powdered (a) adamantane and (b) ferrocene derived from Fourier transformation of the various $\text{FID}_{LPP}(t)$ and $\text{FID}^{\pi}_{LPP}(t)$ in Fig. 6 using a low-power constant RF pulse shape of fixed length $T_p = 2.5$ ms. For $\Theta = \frac{\pi}{2}$ and $\Theta = \pi$, the spectra obtained after low-power excitation (with $T_{\text{Delay}} = 0$ s) were broader than the corresponding $\frac{\pi}{2}$-acquire spectrum (top) in both adamantane and ferrocene with a small "dip" near $\nu \approx 0$ Hz, whereas the corresponding spectra derived from $\text{FID}^{\pi}_{LPP}(t)$ were narrower with a "peak" near $\nu \approx 0$ Hz. With an acquisition delay of $T_{\text{Delay}} = 150$ μs, the "dip" or "peak" remained that increased in intensity with increasing Θ. Scaling factors with respect to the $\frac{\pi}{2}$-acquire spectra are shown next to each spectrum.

To illustrate the effects of a distribution of $\Delta\omega$ on low-power excitation, with and without application of a π_X-pulse, numerical simulations were again performed on an $N_s = 10$ linear spin chain, this time averaged over 200 different spatial configurations such that the average position of the kth spin was given by $\overline{|\vec{r}_k|} = (k-1)d \pm \delta|\vec{r}|$ with $\delta|\vec{r}| \approx 0.06d$. For each $\vec{r}_{\text{spin}}$, the evolution under $\widehat{H}_0 = \widehat{H}_D + \hbar\Delta\omega\widehat{I}_Z$ after low-power excitation from a constant RF pulse was numerically calculated and averaged over 41 different values of $\Delta\omega$ uniformly sampled over $\frac{\Delta\omega}{2\pi} = \pm 10$ Hz. Spectra derived from the calculated $\text{FID}_{LPP}(t)$ and $\text{FID}^{\pi}_{LPP}(t)$ are shown in Fig. 2 for either fixed RF field strength [$\nu_{RF} = 1$ Hz in Figs. 2(a) and 2(b)] or fixed pulse length [$T_p = 250$ ms in Figs. 2(c) and 2(d)]. The (blue) exact spectra along with those calculated using (red) LR [Eq. (11)] and (green) unitarity-corrected LR theory [Eq. (18)] are plotted for $\Theta = 2\pi\nu_{RF}T_p \in \left\{\frac{\pi}{18}, \frac{\pi}{6}, \frac{\pi}{3}, \frac{\pi}{2}, \pi\right\}$. For low-power excitation in the presence of a distribution in $\Delta\omega$, the signal near $\nu \approx 0$ Hz became more negative with increasing Θ in both Figs. 2(a) and 2(c) (see the supplementary material for analogous simulations with $\Delta\omega = 0$). The (red) LR spectra did show a small "dip" near $\nu \approx 0$ Hz but remained relatively unchanged with increasing Θ in Figs. 2(a) and 2(c), whereas the (green) unitarity-corrected LR spectra were closer to the (blue) exact spectra for $\Theta = \frac{\pi}{18}$ and $\Theta = \frac{\pi}{6}$ while exhibiting a more negative "dip" near $\nu \approx 0$ Hz with increasing Θ.

For fixed ν_{RF} in Fig. 2(a), as T_p (and hence Θ) increased, the range of transition frequencies about $\nu \approx 0$ Hz where $\text{sinc}\left(\frac{(\nu^{m,m-1}_{k,j}+\Delta\omega)T_p}{2}\right) > 0$ became narrower. Due to the dispersive and negative signal from transitions with $|\nu^{m,m-1}_{k,j}+\Delta\omega| > 0$ as discussed above, this resulted in a more negative "dip" near $\nu \approx 0$ Hz with increasing Θ. For fixed T_p in Fig. 2(c), as ν_{RF} and hence Θ increased, the contributions from transitions with $\nu^{m,m-1}_{k,j} + \Delta\omega \approx 0$ Hz became smaller due to $\widetilde{V}$. Therefore, the positive signal from transitions with $\nu^{m,m-1}_{k,j} + \Delta\omega \approx 0$ Hz became more attenuated with increasing Θ than the dispersive signals from $|\nu^{m,m-1}_{k,j} + \Delta\omega| > 0$, which led to an increasingly negative "dip" as Θ increased.

The effects of a π_X-pulse after low-power excitation were also simulated. In Figs. 2(b) and 2(d), the (blue) exact spectra derived from the calculated $\text{FID}^{\pi}_{LPP}(t)$ also became more negative for frequencies $|\nu| \leq 20$ Hz with a "peak" being formed at $\nu \approx 0$ Hz with increasing Θ. As expected, the (red) LR spectra were similar to the exact spectra for $\Theta = \frac{\pi}{18}$ but remained relatively unchanged as Θ increased. The (green) unitarity-corrected LR spectra exhibited a similar trend to the exact calculations with increasing Θ. It should be noted that

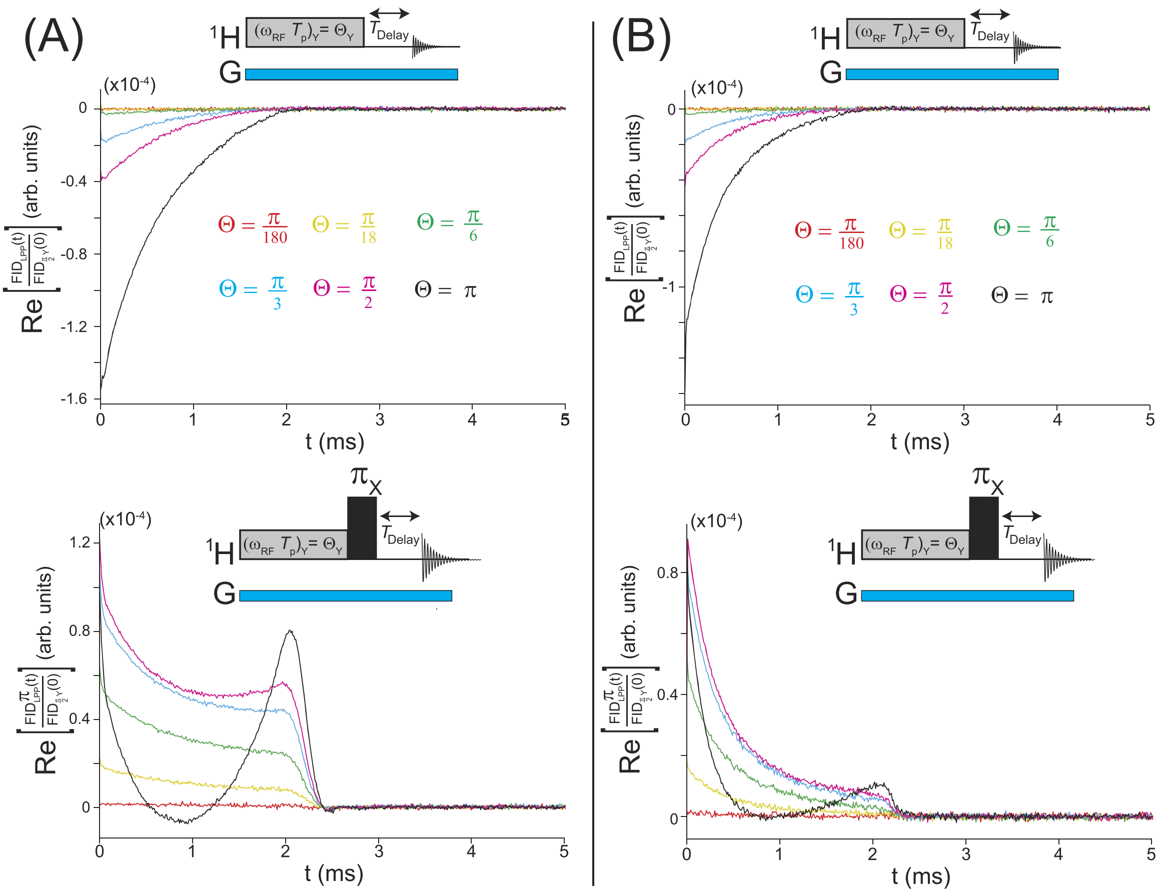

FIG. 8. Experimental $\mathrm{FID}_{LLP}(t)$ and $\mathrm{FID}^{\pi}_{LLP}(t)$ for a constant pulse shape of fixed length ($T_p = 2.5$ ms) in powdered (a) adamantane and (b) ferrocene in the presence of a 0.59 G/cm $\hat{z}$-gradient applied during both excitation and acquisition. All other experimental parameters are identical to those used in Fig. 6. All FIDs, which are plotted with an acquisition delay of $T_{\mathrm{Delay}} = 150\ \mu$s placed after the last RF pulse, are normalized by the first point of the corresponding $\mathrm{FID}_{\frac{\pi}{2}Y}(0)$ in the absence of a gradient.

spectrum obtained by neglecting spectral diffusion during the low-power excitation pulse, i.e., neglecting the second and third terms in Eq. (19), was not significantly different from the exact (green) unitarity-corrected LR spectra in the spin chain simulations (see the supplementary material).

In the presence of nonzero chemical shift differences ($\omega_j \neq \omega_k$ for some spins $j \neq k$), $\widehat{R}_X(\pi)|\varepsilon_{k,m}, d\rangle$ is not directly proportional to $|\varepsilon_{k,-m}, d\rangle$ but instead is given by

$$\widehat{R}_X(\pi)|\varepsilon_{k,m}, d\rangle = \sum_{|\varepsilon_{k',-m},d'\rangle} \left[\widehat{R}_X(\pi)\right]^{\varepsilon_{k,m},d}_{\varepsilon_{k',-m},d'} |\varepsilon_{k',-m}, d'\rangle. \quad (21)$$

Thus when $\widehat{H}_{cs} \neq 0$, $\mathrm{FID}^{LR,\,\mathrm{corr.}}_{LPP}(t)$ can be written as

$$\mathrm{FID}^{\pi,LR\,\mathrm{corr.}}_{LPP}(t) = \frac{\Theta}{2^{N_s} N_s} \left\langle\!\left\langle \sum_{|\varepsilon_{k,m},d\rangle} \sum_{|\varepsilon_{j,m-1,f}\rangle} \sum_{|\varepsilon_{k',m},d'\rangle} \sum_{|\varepsilon_{j',m-1,f'}\rangle} \sum_{|\varepsilon_{l,n-m,c}\rangle} \sum_{|\varepsilon_{p,n-m+1,b}\rangle} \left[\widehat{I}_+\right]^{\varepsilon_{k,m},d}_{\varepsilon_{j,m-1},f} \left[\widehat{I}_-\right]^{\varepsilon_{p,n-m+1},b}_{\varepsilon_{l,n-m},c} \left[\widehat{R}_X(-\pi)\right]^{\varepsilon_{k',-m},d'}_{\varepsilon_{k,m},d} \left[\widehat{R}_X(\pi)\right]^{\varepsilon_{j,m-1},f}_{\varepsilon_{j',1-m},f'} \right.\right.$$
$$\left.\left. \times \left[\widetilde{V}\right]^{\varepsilon_{j',-m+1},f'}_{\varepsilon_{p,n-m+1},b} \left[\widetilde{V}\right]^{\varepsilon_{k',-m},d'}_{\varepsilon_{l,n-m},c} \mathrm{sinc}\!\left(\frac{\left(\omega^{n-m,n-m+1}_{l,p} + \Delta\omega\right)}{2} T_p\right) e^{i\left(\omega^{m,m-1}_{k,j} t + \omega^{-m,1-m}_{k',j'} \frac{T_p}{2}\right)} e^{i\Delta\omega\left(t - \frac{T_p}{2}\right)} \right\rangle\!\right\rangle. \quad (22)$$

While dephasing due to nonzero $\Delta\omega$ is again refocused at $t = \frac{T_p}{2}$, the refocusing of nonzero chemical shift differences is slightly more complex due to the fact that, in general, $\left[\widehat{H}_D, \widehat{H}_{cs}\right] \neq 0$. This non-commutivity was suggested by Khitrin[10,11] to be the origin of "long-lived" signals under low-power excitation followed by a π_X-pulse. The argument of the phase factor in Eq. (22) at time $t = \frac{T_p}{2}$ is given by

$$\frac{T_p}{2}\left(\omega^{m,m-1}_{k,j} + \omega^{-m,1-m}_{k',j'}\right), \quad (23)$$

which is in general nonzero and contains contributions from both $\widehat{H}_D$ and $\widehat{H}_{cs}$, the latter of which is only partially refocused due to a π_X-pulse. As a result, less refocusing occurs when

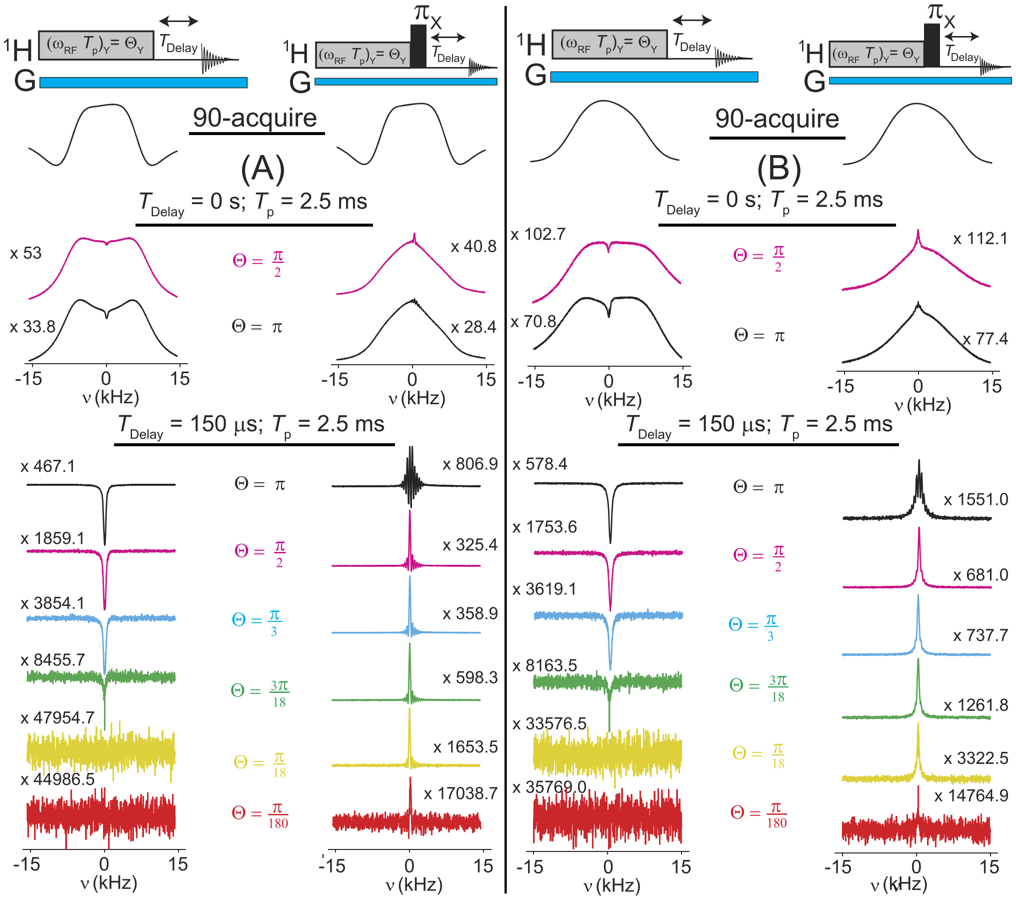

FIG. 9. Experimental spectra of powdered (a) adamantane and (b) ferrocene derived from Fourier transformation of the various $\text{FID}_{LPP}(t)$ and $\text{FID}^{\pi}_{LPP}(t)$ in Fig. 8 using a low-power constant RF pulse shape of fixed length T_p = 2.5 ms in the presence of a 0.59 G/cm gradient applied along the $\hat{z}$-direction during both excitation and acquisition. All other experimental parameters were the same as those used in Fig. 7. While the intensities appeared slightly lower, in general, the small resonance at ν = 1.74 kHz was not observed in the presence of a gradient. Scaling factors with respect to the $\frac{\pi}{2}$-acquire spectra (in the absence of a gradient) are shown next to each spectrum.

$\left[\widehat{H}_D, \widehat{H}_{cs}\right] \neq 0$ at time $t = \frac{T_p}{2}$ in Eq. (22) compared to the case when $\widehat{H}_{cs} = 0$ in Eq. (20).

For completeness, we also consider low-power excitation in the weak coupling limit when $|\omega_{j,cs} - \omega_{k,cs}| \gg |\omega_{D,jk}|$. In the weak coupling limit, the flip-flop terms in $\widehat{H}_D$ [Eq. (3)] can be safely ignored, i.e., $\widehat{H}_D \approx \hbar \sum_{k<j} 2\omega_{D,k,j}\widehat{I}_{Z,k}\widehat{I}_{Z,j}$. As a result, $\left[\widehat{H}_D, \widehat{H}_{cs}\right] = 0$. In the weak coupling limit, the states $|\varepsilon_{k,m}, d\rangle$ are simultaneous eigenstates of both $\widehat{H}_D$ and $\widehat{H}_{cs}$ with $\widehat{H}_D|\varepsilon_{k,m}, d\rangle = \varepsilon_{D,k,|m|}|\varepsilon_{k,m}, d\rangle$, $\widehat{H}_{cs}|\varepsilon_{k,m}, d\rangle = \varepsilon_{cs,k,m}|\varepsilon_{k,m}, d\rangle$, and $\left(\widehat{H}_D + \widehat{H}_{cs}\right)|\varepsilon_{k,m}, d\rangle = \varepsilon_{k,m}|\varepsilon_{k,m}, d\rangle$, where $\varepsilon_{k,m} = \varepsilon_{D,k,|m|} + \varepsilon_{cs,k,m}$. Furthermore, $|\varepsilon_{k,-m}, f\rangle = \widehat{R}_X(\pi)|\varepsilon_{k,m}, f\rangle$, with $\varepsilon_{k,-m} = \varepsilon_{D,k,|m|} - \varepsilon_{cs,k,m}$.

In the weak-coupling limit, $\text{FID}^{\pi,LR,\text{corr.}}_{LPP}(t)$ reduces to

$$\text{FID}^{\pi,LR\,\text{corr.}}_{LPP}(t) = \frac{\Theta}{2^{N_s}N_s}\left\langle\!\!\left\langle \sum_{|\varepsilon_{k,m},d\rangle}\ \sum_{|\varepsilon_{j,m-1,f}\rangle}\ \sum_{|\varepsilon_{l,n-m,c}\rangle}\ \sum_{|\varepsilon_{p,n-m+1,b}\rangle} \left[\widehat{I}_+\right]^{\varepsilon_{k,m},d}_{\varepsilon_{j,m-1},f} \left[\widehat{I}_-\right]^{\varepsilon_{p,n-m+1},b}_{\varepsilon_{l,n-m},c} \left[\widetilde{V}\right]^{\varepsilon_{j,-m+1},f}_{\varepsilon_{p,n-m+1},b} \left[\widetilde{V}\right]^{\varepsilon_{k,-m},d}_{\varepsilon_{l,n-m},c} \right.\right.$$
$$\left.\left. \times \operatorname{sinc}\left(\frac{\left(\omega^{n-m,n-m+1}_{l,p} + \Delta\omega\right)}{2}T_p\right) e^{i\omega^{m,m-1}_{D,k,j}\left(t+\frac{T_p}{2}\right)} e^{i\left(\omega^{m,m-1}_{cs,k,j}+\Delta\omega\right)\left(t-\frac{T_p}{2}\right)} \right\rangle\!\!\right\rangle, \tag{24}$$

where $\omega^{m,m-1}_{D,k,j} = \frac{\varepsilon_{D,k,|m|}-\varepsilon_{D,j,|m-1|}}{\hbar}$ and $\omega^{m,m-1}_{cs,k,j} = \frac{\varepsilon_{cs,k,m}-\varepsilon_{cs,j,m-1}}{\hbar}$. In this case, the inhomogeneous broadening under both $\widehat{H}_{cs}$ and $\Delta\omega$ is refocused at $t = \frac{T_p}{2}$ for a constant low-power pulse shape [Eq. (24)] after which dephasing due to both $\widehat{H}_{cs} \neq 0$ and $\Delta\omega$ proceeds for an additional time $\frac{T_p}{2}$ such that the amount of dephasing due to both nonzero $\widehat{H}_{cs}$ and $\Delta\omega$ is identical at $t = T_p$ as it was at $t = 0$. In this case, the commutivity of $\widehat{H}_D$ and $\widehat{H}_{cs}$, which is due to neglecting the flip-flop terms of $\widehat{H}_D$ in

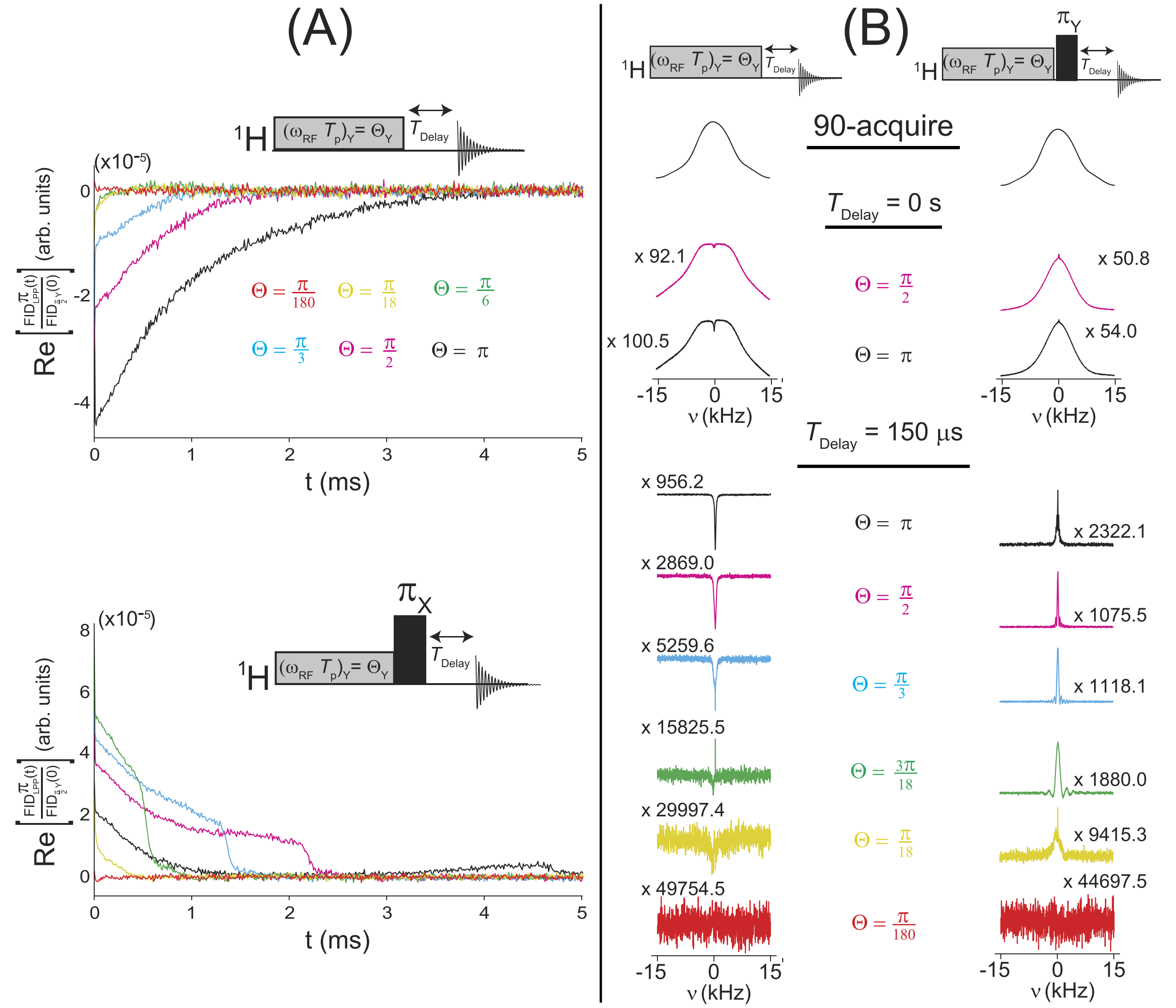

FIG. 10. (a) Experimental FID$_{LLP}(t)$ and FID$^{\pi}_{LLP}(t)$ for fixed ν_{RF} = 100 Hz in powdered hexamethylbenzene using constant low-power excitation ($\frac{\omega_{RF}(t)}{2\pi}$ = 100 Hz for $0 \le t \le T_p$) for "nominal" flip-angles of $\Theta = 2\pi\nu_{RF}T_p \in \left\{\frac{\pi}{180}, \frac{\pi}{18}, \frac{\pi}{6}, \frac{\pi}{3}, \frac{\pi}{2}, \pi\right\}$. All FIDs, which are plotted with an acquisition delay of $T_{\rm Delay}$ = 150 μs placed after the last RF pulse, are normalized by the first point of FID$_{\frac{\pi}{2}Y}(0)$. (b) Corresponding spectra derived from Fourier transformation of the various FID$_{LPP}(t)$ and FID$^{\pi}_{LPP}(t)$ in Fig. 10(a). For $\Theta = \frac{\pi}{2}$ and $\Theta = \pi$, the spectra obtained after low-power excitation (with $T_{\rm Delay}$ = 0 s) were broader than the $\frac{\pi}{2}$-acquire spectrum (top) with a small "dip" near $\nu \approx 0$ Hz, whereas the corresponding spectra derived from FID$^{\pi}_{LPP}(t)$ were narrower with a very small "peak" near $\nu \approx 0$ Hz. With an acquisition delay of $T_{\rm Delay}$ = 150 μs, the spectra derived from FID$_{LPP}(t)$ were dominated by a "dip" near $\nu \approx 0$ Hz for $\Theta \ge \frac{\pi}{3}$. For $\Theta \ge \frac{\pi}{18}$, the spectra derived from FID$^{\pi}_{LPP}(t)$ consisted of positive peak near $\nu \approx 0$ Hz with wiggles due to the "box"-like nature of FID$^{\pi}_{LPP}(t)$ in Fig. 10(a).

Eq. (3), results in a greater amount of signal being refocused than when $\left[\widehat{H}_{cs}, \widehat{H}_D\right] \neq 0$ in Eq. (21).

III. EXPERIMENT

The experimental results shown in Figs. 3–12 were performed at room temperature (T = 298 K) on a 500 MHz Bruker AVANCE NMR spectrometer equipped with a TCI 500S2 H-C/N-D-05 Z Bruker cryoprobe. The chemicals adamantane (99% purity), ferrocene (98% purity), and hexamethylbenzene (99% purity) were obtained from Sigma-Aldrich Company, Ltd. and used without further purification. In preparing powdered samples, chemicals were ground in a mortar and pestle and placed in regular 5 mm Ultra Precision NMR tubes (rated to 600 MHz, Norell, Inc.). Single-crystalline samples of adamantane and ferrocene were obtained by slow sublimation of the powdered chemical placed inside a test tube buried in a sand bath overnight. Crystals that grew on the tube wall were collected, and only those crystals without any noticeable defects under a microscope were used in the experiments. Crystals were placed in a 5 mm D_2O susceptibility matched Shigemi tube without determining crystal orientation. The high-power RF field strengths for the hard $\frac{\pi}{2}$- and π-pulses were ν_{RF} = 29.50 kHz, ν_{RF} = 29.65 kHz, and ν_{RF} = 29.48 kHz for adamantane, ferrocene, and hexamethylbenzene, respectively. Unless otherwise noted, all experiments were carried out by first locking and shimming on a D_2O sample prior to placing each solid sample into the magnet. Additional experiments on low-power excitation on powdered hexamethylbenzene were also carried out on a 400 MHz Bruker AVANCE III HD spectrometer and are given in the supplementary material. All experiments in Figs. 3–12 were acquired using the following parameters: dwell time of Δt = 10 μs, N_{pts} = 4096 complex data points, 64 scans, and a relaxation delay of

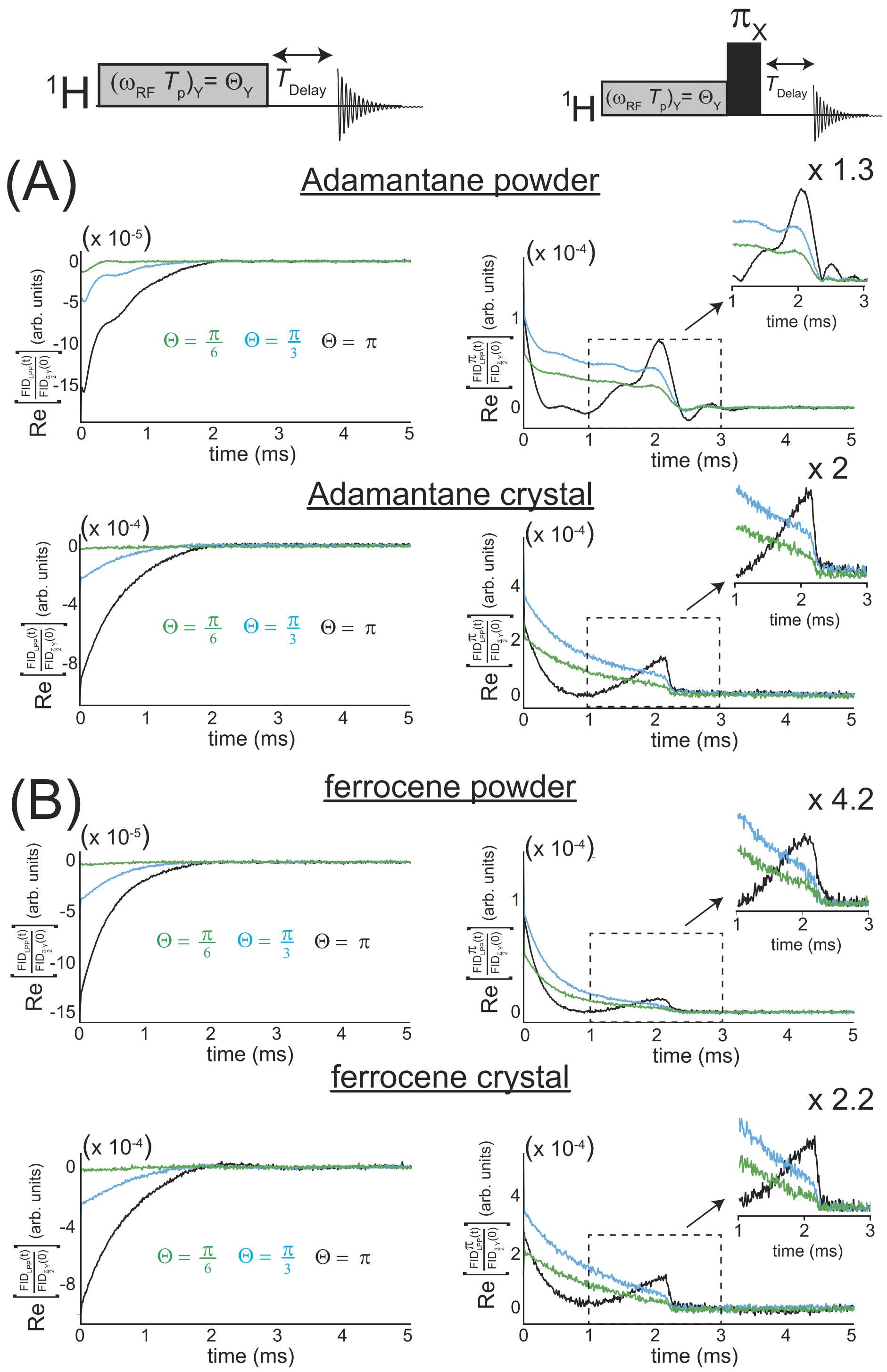

FIG. 11. Experimental $\text{FID}_{LPP}(t)$ and $\text{FID}^{\pi}_{LPP}(t)$ for fixed $T_p = 2.5$ ms in both powdered and single-crystalline (a) adamantane and (b) ferrocene using constant, low-power excitation for "nominal" flip-angles of $\Theta = \frac{\pi}{6}$ ($\nu_{RF} \approx 33$ Hz), $\Theta = \frac{\pi}{3}$ ($\nu_{RF} \approx 67$ Hz), and $\Theta = \pi$ ($\nu_{RF} = 200$ Hz). All FIDs, which were plotted with an acquisition delay of $T_{\text{Delay}} = 150\ \mu$s placed after the last RF pulse, were normalized by the first point of the corresponding $\text{FID}_{\frac{\pi}{2}}(0)$. An inset centered at $t \approx T_p = 2$ ms is shown where the various $\text{FID}^{\pi}_{LPP}(t)$ suddenly decay to zero.

$d_1 = 30$ s. Spectra were analyzed and plotted using a combination of Topspin, MATLAB,[19] and the open source Python package Nmrglue.[20]

IV. RESULTS AND DISCUSSION

In the following, experimental results on low-power excitation in powdered adamantane, ferrocene, and hexamethylbenzene samples and in single-crystalline adamantane and ferrocene samples are presented. In most cases, the corresponding FIDs and spectra are given for different values of Θ under conditions of either fixed ν_{RF} or T_p. Discussions relating the experimental results to the numerical and theoretical results presented in Sec. II are given along with a comparison to low-power excitation in inhomogeneously broadened spin systems.[14]

A. Low-power excitation for fixed ν_{RF} in powdered adamantane and ferrocene

In Figs. 3–5, experimental results, with and without the application of a π_X-pulse after low-power excitation, are presented for powdered adamantane and ferrocene. In Fig. 3, the

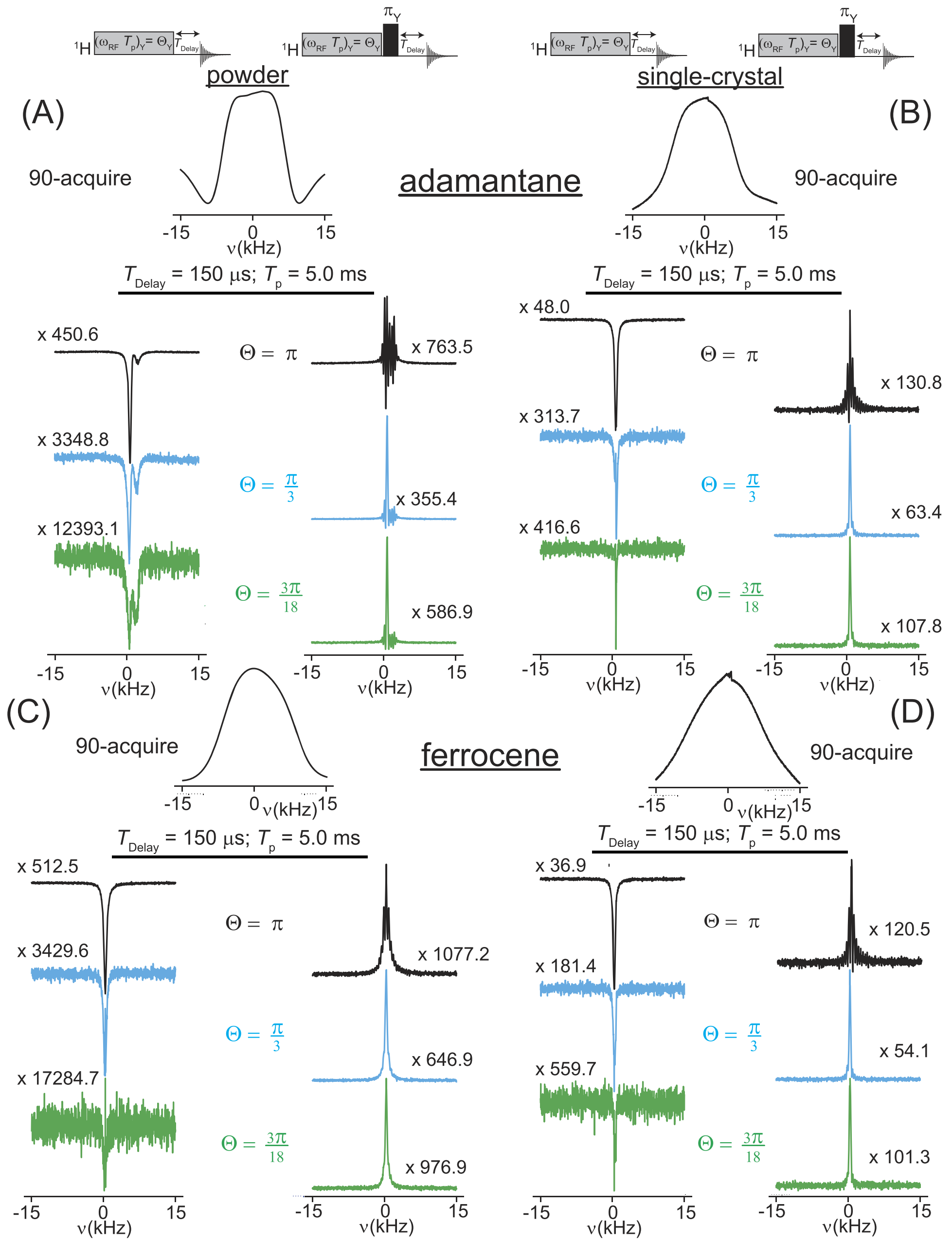

FIG. 12. Experimental spectra for both powdered and single-crystalline (a) adamantane and (b) ferrocene samples derived from Fourier transformation of the various FIDs given in Fig. 11. The corresponding $\frac{\pi}{2}$-acquire spectra are shown at the top. (a) The resonance at $\nu \approx 1.74$ kHz observed in powdered adamantane was not observed in single-crystalline adamantane. The low-power excitation spectra for powdered adamantane were broader than the corresponding low-power excitation spectra for single-crystalline adamantane. The "peak" in the spectra derived from $\text{FID}^{\pi}_{LPP}(t)$ in Fig. 11(a) was similar in both powdered and single-crystalline samples. (b) There were no significant differences in the spectra between single-crystalline and powdered ferrocene. Scaling factors with respect the corresponding $\frac{\pi}{2}$-acquire spectra are shown next to each spectrum.

experimental FIDs for $\nu_{RF} = 100$ Hz and $\Theta = 2\pi\nu_{RF}T_p$ ranging from $\Theta = \frac{\pi}{180}\left[T_p = 27.8\,\mu\text{s}\right]$ to $\Theta = \pi\left[T_p = 5\,\text{ms}\right]$ are shown for both constant ($\omega_{RF}(t) = 2\pi\nu_{RF}$ for $0 \le t \le T_p$) and ramped ($\omega_{RF}(t) = \frac{4\pi\nu_{RF}t}{T_p}$ for $0 \le t \le T_p$) RF pulse shapes. The FIDs with an acquisition delay of $T_{\text{Delay}} = 150\,\mu$s placed after the last RF pulse are plotted in Fig. 3. The signals using a ramped pulse shape were 3-4 times larger than the signals using a constant pulse shape. In both [Fig. 3(a)] adamantane and [Fig. 3(b)] ferrocene, $\text{FID}_{LPP}(t)$ became increasingly negative and decayed more slowly with increasing Θ (i.e., increasing T_p). The FIDs also lasted a time $t \approx T_p$ after the last RF pulse, which is consistent with the notion of coherent transients[21] observed in inhomogeneously broadened systems. After application of a π_X-pulse, $\text{FID}^{\pi}_{LPP}(t)$ resembled the time-reversed shape[22] of the low-power excitation pulse, which was either "box"-like or "triangle"-like for the constant and ramped pulse shapes, respectively (see the supplementary material for more details). This behavior was also similar to that observed in inhomogeneously broadened spin systems.[14]

The corresponding spectra obtained by Fourier transformation of the FIDs in Fig. 3 are given in Figs. 4 and 5 for the constant and ramped pulse shapes, respectively. In powdered adamantane, a small additional signal was observed in the low-power excitation experiments at a chemical shift of $\delta = 3.476$ ppm from the center of the adamantane spectrum ($\nu \approx 1.74$ kHz in Figs. 4 and 5). A similar spectral signature was previously obeved for Carr-Purcell-Meiboom-Gill pulse train experiments on powdered adamantane.[23] While the exact nature of this resonance is not known, it is shown in this work that in the presence of a magnetic field gradient (Figs. 8 and 9) and for single crystalline adamantane samples (Figs. 11 and 12), this extra resonance at $\nu \approx 1.74$ kHz was not observed in the low-power excitation spectrum. For a constant pulse shape, a small "dip" or "peak" was generated near the RF transmitter frequency ($\nu \approx 0$ Hz, which was chosen to be near the center of the $\frac{\pi}{2}$-acquire spectrum) for low-power excitation and low-power excitation followed by a π_X-pulse, respectively. This was particularly noticeable for $\Theta = \frac{\pi}{2}$ and $\Theta = \pi$, as shown in Fig. 4. For the spectra after application of a π_X-pulse, there appeared wiggles near $\nu \approx 0$ Hz due to the "box"-like shape of $\text{FID}^{\pi}_{LPP}(t)$ in Fig. 3. With an acquisition delay of $T_{\text{Delay}} = 150\ \mu$s, only a "dip" or a "peak" near $\nu \approx 0$ Hz remained in the spectrum that became more pronounced with increasing Θ. This is related to the observation[15] that delayed-acquisition highlights sharp spectral features in inhomogeneously broadened spectra (see Appendix A for more details).

For a ramped pulse shape, the corresponding spectra (Fig. 5) derived from $\text{FID}_{LPP}(t)$ for both powdered adamantane and ferrocene exhibited similar behavior to that found using a constant pulse shape (Fig. 4). Since $\text{FID}^{\pi}_{LPP}(t)$ gradually tended to zero as $t \rightarrow T_p$ for a ramped pulse shape (compared with the "abrupt" decay of $\text{FID}^{\pi}_{LPP}(t)$ at $t \approx T_p$ for a constant pulse shape), the corresponding spectra did not exhibit "wiggles" and were broader than the spectra using a constant pulse shape (Fig. 4).

Overall, the results in Figs. 3–5 were consistent with the numerical simulations in Figs. 1, 2(a), and 2(b), although the "dips" and "peaks" were more pronounced in the toy model used in Figs. 1 and 2. This is likely due to the finite spin system size ($N_s = 10$) used in the simulations, differences in coupling networks (linear vs. nonlinear spin arrangements), orientational effects of $\widehat{H}_D$, and neglect of correlations between anisotropic inhomogeneous broadening (ABMS, CSA, chemical shift differences, B_0 inhomogeneity, etc.) and $\widehat{H}_D$. It should also be noted that the results in Figs. 3–5 were similar to previous experimental results in inhomogeneously broadened spin systems.[14]

B. Low-power excitation for fixed T_p in powdered adamantane and ferrocene samples

While the previous discussion focused on fixed ν_{RF}, experiments were also performed for a constant pulse shape of fixed length, $T_p = 2.5$ ms. In this case, different Θ values were achieved by varying ν_{RF} from $\nu_{RF} = 2$ Hz (for $\Theta = \frac{\pi}{180}$) to $\nu_{RF} = 200$ Hz (for $\Theta = \pi$). The corresponding FIDs and spectra are given in Figs. 6 and 7, respectively. Under low-power excitation with fixed T_p, a "dip" again appeared near $|\nu| \approx 0$ Hz that increased in intensity with increasing Θ in both adamantane and ferrocene. $\text{FID}^{\pi}_{LPP}(t)$ again had a "box"-like shape that abruptly decayed to zero at $t \approx T_p = 2.5$ ms with the corresponding spectra consisting of a "peak" at $\nu \approx 0$ Hz that increased in intensity with increasing Θ. The spectra in Fig. 7 are consistent with the numerical simulations in Figs. 2(c) and 2(d) and with previous experimental results in inhomogeneously broadened spin systems.[14]

C. Effects of a magnetic field gradient in powdered adamantane and ferrocene

The constant time excitation experiments shown in Figs. 6 and 7 were also performed in the presence of a 0.59 G/cm $\widehat{z}$-gradient applied during both low-power excitation and acquisition, with the FIDs and corresponding spectra given in Figs. 8 and 9, respectively. For adamantane, the small residual peak at $\nu = 1.74$ kHz was not observed in the low-power excitation spectra [Fig. 9(a)], indicating that this signal was dephased by the applied gradient. The $\frac{\pi}{2}$-acquire spectra, with and without a gradient, were nearly identical to each other (Fig. 7 vs. Fig. 9). In fact, with exception of the adamantane signal at $\nu \approx 1.74$ kHz, the "dip" and "peaks" generated by low-power excitation, with or without an applied magnetic field gradient, were also nearly identical with a slight decrease in intensity due to the magnetic field gradient. Furthermore, spectra for low-power excitation under conditions of constant ν_{RF}, with and without the application of a magnetic field gradient, were also nearly identical [again, with the exception of the adamantane resonance at $\nu \approx 1.74$ kHz that was removed by the gradient (data not shown)].

D. Low-power excitation for fixed ν_{RF} in powdered hexamethylbenzene

As shown in Figs. 3 and 6, $\text{FID}^{\pi}_{LPP}(t)$ for both adamantane and ferrocene exhibited "echo"-like phenomena after application of a π_X-pulse. As mentioned in Sec. II, a π_X-pulse cannot refocus dipolar dephasing but can completely refocus inhomogeneous dephasing due to ABMS, CSA, and B_0 inhomogeneity. However, dephasing due to nonzero chemical shift differences is only partially refocused by a π_X-pulse due to the fact that, in general, $\left[\widehat{H}_D, \widehat{H}_{cs}\right] \neq 0$. While it has been previously noted[9] that local offsets (say, from ABMS) can be trivially refocused by a π_X-pulse after low-power excitation in solids, it was argued[9–11] that the "long-lived" signals generated by a π_X-pulse after low-power excitation were a result of the non-commutivity of $\widehat{H}_D$ and $\widehat{H}_{cs}$. As a result, the "long-lived" signals previously observed in adamantane[9,10] were thought to be a new type of echo due to small isotropic chemical shift differences between the two types of protons in adamantane. A simplified three-state model[9,10] and numerical simulations[11] were provided as theoretical justification.

In Figs. 3(b) and 6(b), "long-lived" signals were also observed in ferrocene where there are no nonzero isotropic chemical shift differences. However, the unit cell for ferrocene does consist of two inequivalent ferrocene molecules that are oriented in such a way that the ^{1}H spins on different molecules within a unit cell can exhibit, due to CSA, a nonzero chemical shift difference that depends upon crystallite orientation.[24] Thus the "long-lived" signal observed in $\text{FID}^{\pi}_{LPP}(t)$ for powdered ferrocene could still be consistent with the previous theoretical model[9,10] requiring nonzero, effective chemical shift differences to generate this new kind of echo in dipolar solids.

One prior piece of evidence for the need of nonzero chemical shift differences to observe "long-lived" signals in dipolar solids was the reported absence of "long-lived" signal in hexamethylbenzene.[10] Unlike ferrocene, hexamethylbenzene has only one molecule per unit cell[25] and exhibits fast methyl and ring rotations at room temperature.[26] As a result, there are no effective chemical shift differences between any ^{1}H spins within a hexamethylbenzene molecule, and all ^{1}H spins within a unit cell resonate at the same frequency. Contrary to prior observations,[10] experiments on powdered hexamethylbenzene show both *nonzero* $\mathrm{FID}_{LPP}(t)$ and $\mathrm{FID}^{\pi}_{LPP}(t)$ for fixed $\nu_{RF} = 100$ Hz in Fig. 10(a) for $\Theta \in \left\{\frac{\pi}{180}, \frac{\pi}{18}, \frac{\pi}{6}, \frac{\pi}{3}, \frac{\pi}{2}, \pi\right\}$. For $\Theta \geq \frac{\pi}{3}$, a "dip" near $\nu \approx 0$ Hz was clearly observed in the low-power excitation spectra. For low-power excitation followed by a π_X-pulse, the spectra became narrower with increasing Θ up to $\Theta = \frac{\pi}{2}$ (for $\Theta = \pi$, the spectra were a little wider and also smaller compared with $\Theta = \frac{\pi}{2}$). Similar to the results in Fig. 3 for both powdered ferrocene and adamantane, the "box"-like shape of $\mathrm{FID}^{\pi}_{LPP}(t)$ in Fig. 10 indicates that a π_X-pulse is able to refocus inhomogeneous dephasing in hexamethylbenzene. Since there are no nonzero chemical shift differences, the inhomogeneous dephasing that is being refocused in hexamethylbenzene is likely to due to ABMS, CSA, and/or B_0 inhomogeneity. It should be noted that similar results in powdered hexamethylbenzene were also observed at a 400 MHz field strength (see the supplementary material).

E. Low-power excitation in single crystals of ferrocene and adamantane at fixed T_p = 2.5 ms

The various $\mathrm{FID}^{\pi}_{LPP}(t)$ shown in Fig. 10 for powdered hexamethylbenzene suggest that a π_X-pulse applied after low-power excitation refocuses differences in CSA and ABMS,[12,13] which vary due to the distribution of crystallite orientations and/or sizes within the sample and the effects of B_0 inhomogeneity. Single-crystalline samples, on the other hand, should not exhibit significant ABMS or CSA broadening due to the fact that only one orientation (or a small number if the crystal has defects) is present. To test the effects of ABMS and CSA broadening on $\mathrm{FID}^{\pi}_{LPP}(t)$, experiments were performed on both powdered and single-crystalline samples of adamantane and ferrocene placed in a 5 mm Shigemi tube. The various $\mathrm{FID}_{LPP}(t)$ and $\mathrm{FID}^{\pi}_{LPP}(t)$ for $\Theta \in \left\{\frac{\pi}{6}, \frac{\pi}{3}, \pi\right\}$ for $T_p = 2.5$ ms along with the corresponding spectra are given in Figs. 11 and 12, respectively. Both $\mathrm{FID}_{LPP}(t)$ and $\mathrm{FID}^{\pi}_{LPP}(t)$ appeared different between powdered and single-crystalline adamantane samples, which was mainly due to the absence of the resonance at $\nu = 1.74$ kHz in the single-crystalline data [Fig. 12(a)]. For $\Theta = \frac{\pi}{3}$, there did appear a small splitting of $\Delta\nu \approx -270$ Hz in the spectrum derived from $\mathrm{FID}_{LPP}(t)$ in Fig. 12(a) in single-crystalline adamantane [which could be removed by application of a magnetic field gradient (data not shown)]. The low-power excitation spectra were similar between both powdered and single crystalline ferrocene (Fig. 12). In all samples, the edge of $\mathrm{FID}^{\pi}_{LPP}(t)$ at $t \approx T_p$ was relatively sharp [as highlighted in the insets given in Fig. 11(a)], which suggests that the inhomogeneous broadening in both powdered (due to B_0 inhomogeneity, CSA, and/or ABMS) and single-crystalline (mainly due to B_0 inhomogeneity and/or crystal defects) samples was likely larger than the low-power RF pulse strength (which varied from $\nu_{RF} = 33.33$ Hz for $\Theta = \frac{\pi}{6}$ to $\nu_{RF} = 200$ Hz for $\Theta = \pi$) although the single crystalline samples both appeared to have sharper drops in $\mathrm{FID}^{\pi}_{LPP}(t)$ at $t \approx T_p$ relative to the corresponding powdered samples. This is consistent with numerical simulations of inhomogeneously broadened spin systems, which demonstrate that the signal for $\mathrm{FID}^{\pi}_{LPP}(t)$ at $t \approx T_p$ is larger for $\Theta = \pi$ than for $\Theta = \frac{\pi}{3}$ and $\Theta = \frac{\pi}{6}$ when $\Delta\omega_{\frac{1}{2}} \gg \omega_{RF}$ (see the supplementary material).

V. CONCLUSIONS

In this work, the previous theory for low-power RF excitation of inhomogeneously broadened spin systems[14] was applied to the problem of low-power RF excitation in homogeneously broadened dipolar solids. In the linear response regime, the interaction with the RF excitation pulse of length T_p is only taken to first-order; as a result, the homogeneous nature of dipolar solids was not evident in the linear response results. However, for transition frequencies $|\nu| \leq \nu_{RF}$, the RF interaction represents a strong perturbation that cannot be accurately treated within the linear response regime. Similar to the inhomogeneous case,[14] a unitarity-corrected linear response propagator was shown to give results that were closer to exact calculations by attenuating the signal intensity from transitions $|\nu| \leq \nu_{RF}$, resulting in lower spectral intensity at the applied RF transmitter frequency, $\nu \approx 0$ Hz. In simulations shown in Fig. 2 and in experiments on adamantane, ferrocene, and hexamethylbenzene shown in Figs. 3–12, the spectra after low-power excitation contained a "dip" at $\nu \approx 0$ Hz that increased in intensity with increasing nominal flip-angle Θ. In the absence of nonzero chemical shift differences, application of a π_X-pulse after low-power excitation refocuses the inhomogeneous dephasing in powdered samples due to B_0 inhomogeneity, anisotropic bulk magnetic susceptibility (ABMS), and/or chemical shift anisotropy (CSA) at a time $t = \frac{T_p}{2}$ after the π_X-pulse. In the presence of nonzero chemical shift differences, however, there is only a partial refocusing of inhomogeneous dephasing due to the fact that the dipolar and chemical shift interactions do not commute with one another; only in the weak-coupling limit will all inhomogeneous dephasing be completely refocused at $t = \frac{T_p}{2}$. While previous work[9–11] has suggested that nonzero chemical shift differences are necessary to observe an echo after application of a π_X-pulse in dipolar solids, "long-lived" signals were observed in powdered hexamethylbenzene, where all ^{1}H spins within a unit cell resonate at the same frequency. Further experiments in powdered and single-crystalline adamantane and ferrocene samples indicate that the refocusing of B_0 inhomogeneity, ABMS, and/or CSA is the dominant contribution to the "long-lived" signal observed after an application of a π_X-pulse.

For future work, pulse sequences that can enhance the "dips" under low-power excitation, say, using low-power sinc pulses, are being developed. Since the behavior under low-power excitation in dipolar solids was similar to that observed for inhomogeneously broadened systems,[14] further work is also being performed to explore the boundaries between homogeneous and inhomogeneous behavior in dipolar solids, in particular, addressing the question under what conditions an RF pulse sequence could "burn a hole" in dipolar systems. Low-power excitation of dipolar systems can also be used for selective spatial excitation in solid-state MRI applications.[11,27] Furthermore, low-power excitation in dipolar systems could be used to measure diffusion[3] in plastic crystals such as adamantane or for molecules in liquid crystalline environments.

SUPPLEMENTARY MATERIAL

In supplementary material, the nature of $\widetilde{V}$ in the unitarity-corrected LR propagator in Eq. (14) and when it is safe to neglect spectral diffusion during the low-power pulse are examined. Additional simulations on a linear spin chain are also provided, along with a discussion of the effects of the amount of inhomogeneous broadening relative to ν_{RF} on the behavior of $\mathrm{FID}^{\pi}_{LPP}(t)$ near times $t = T_p$ is given. The connection between the RF pulse shape, ω_{RF}, and $\mathrm{FID}^{\pi,LR}_{LPP}(t)$, along with additional experiments on powdered hexamethylbenzene, are also presented. Finally, pulse programs used in this work are provided.

ACKNOWLEDGMENTS

We would like to dedicate this work to the memory of Dr. Anatoly Khitrin. We acknowledge support from the National Science Foundation under Nos. CHE-1056846, CHE-1626015, and CHE-1807724. Some of the numerical simulations were conducted using resources of the University of Miami Center for Computational Science.

APPENDIX A: DESCRIBING THE FID FOR AN ARBITRARY SPIN SYSTEM IN TERMS OF AN INHOMOGENEOUS DISTRIBUTION OF NON-INTERACTING SPINS

In the following, we show by construction that the FID for an arbitrary spin system can always be described by an equivalent inhomogeneously broadened system of *non-interacting* spins ($I = \frac{1}{2}$) with a (possibly complex) frequency distribution function, $g(\omega)$. Consider a system of *interacting* spins ($I = \frac{1}{2}$) with a Hamiltonian $\widehat{H}$ such that $\left[\widehat{H}, \widehat{I}_Z\right] = 0$. As such, we can define simultaneous eigenstates of $\widehat{H}$ and $\widehat{I}_Z$, $|\varepsilon_{q,m}, f\rangle$, with $\widehat{H}|\varepsilon_{q,m}, f\rangle = \varepsilon_{q,m}|\varepsilon_{q,m}, f\rangle$ and $\widehat{I}_Z|\varepsilon_{q,m}, f\rangle = m|\varepsilon_{q,m}, f\rangle$. The indices f and $g \neq f$ for the states $|\varepsilon_{q,m}, f\rangle$ and $|\varepsilon_{q,m}, g\rangle$ denote different degenerate states with respect to $\widehat{H}$ and $\widehat{I}_Z$ such that $\langle\varepsilon_{q,m}, f|\varepsilon_{p,n}, g\rangle = \delta_{qp}\delta_{mn}\delta_{fg}$, where δ_{ij} is the Kronecker delta function with $\delta_{ii} = 1$ and $\delta_{ij} = 0$ for $j \neq i$.

For an arbitrary initial state, $\widehat{\rho}(0)$, the $\mathrm{FID}(t) = \langle\widehat{I}_+(t)\rangle$ at times $t = k\Delta t$ for $k = 0$ to $k = N_{pts} - 1$ is given by

$$\begin{aligned}\mathrm{FID}(k\Delta t) &= \mathrm{Trace}\left[\widehat{I}_+\widehat{U}(k\Delta t)\widehat{\rho}(0)\widehat{U}^{\dagger}(k\Delta t)\right]\\ &= \sum_{|\varepsilon_{p,m},d\rangle}\sum_{|\varepsilon_{q,m-1},f\rangle}\left[\widehat{I}_+\right]^{\varepsilon_{p,m},d}_{\varepsilon_{q,m-1},f}\left[\widehat{\rho}(0)\right]^{\varepsilon_{q,m-1},f}_{\varepsilon_{p,m},d}e^{i\omega^{m}_{p,q}k\Delta t}\\ &\equiv \int_{-\frac{\pi}{\Delta t}}^{\frac{\pi}{\Delta t}} \mathrm{d}\omega[g(\omega)]e^{ik\omega\Delta t}, \qquad \text{(A1)}\end{aligned}$$

where $\widehat{U}(k\Delta t) = \exp\left(-i\frac{\widehat{H}}{\hbar}k\Delta t\right)$ and $g(\omega)$ is the (possibly complex) frequency distribution for the effective non-interacting spins. Assume that Δt is chosen such that the spectrum of $\widehat{H}$ for the observable $\widehat{I}_+$ falls entirely within the range $-\frac{\pi}{\Delta t} \leq \omega \leq \frac{\pi}{\Delta t}$.

Decomposing $g(\omega)$ into its Fourier series,

$$\begin{aligned}g(\omega) &= \sum_{n=0}^{\infty}(A_n\cos(n\omega\Delta t) + B_n\sin(n\omega\Delta t)),\\ A_0 &= \frac{\Delta t}{\pi}\int_{-\frac{\pi}{\Delta t}}^{\frac{\pi}{\Delta t}} d\omega g(\omega)\\ &= \frac{\Delta t}{2\pi}\sum_{|\varepsilon_{p,m},d\rangle}\sum_{|\varepsilon_{q,m-1},f\rangle}\left[\widehat{I}_+\right]^{\varepsilon_{p,m},d}_{\varepsilon_{q,m-1},f}\left[\widehat{\rho}(0)\right]^{\varepsilon_{q,m-1},f}_{\varepsilon_{p,m},d},\\ B_0 &= 0,\\ A_n &= \frac{\Delta t}{2\pi}\int_{-\frac{\pi}{\Delta t}}^{\frac{\pi}{\Delta t}} d\omega g(\omega)\cos(n\omega\Delta t)\\ &= \frac{\Delta t}{2\pi}\left(\sum_{|\varepsilon_{p,m},d\rangle}\sum_{|\varepsilon_{q,m-1},f\rangle}\left[\widehat{I}_+\right]^{\varepsilon_{p,m},d}_{\varepsilon_{q,m-1},f}\left[\widehat{\rho}(0)\right]^{\varepsilon_{q,m-1},f}_{\varepsilon_{p,m},d}e^{i\omega^{m}_{p,q}n\Delta t}\right)\\ &\quad + h.c.,\\ B_n &= \frac{\Delta t}{2\pi}\int_{-\frac{\pi}{\Delta t}}^{\frac{\pi}{\Delta t}} d\omega g(\omega)\sin(n\omega\Delta wt)\\ &= -i\frac{\Delta t}{2\pi}\left(\sum_{|\varepsilon_{p,m},d\rangle}\sum_{|\varepsilon_{q,m-1},f\rangle}\left[\widehat{I}_+\right]^{\varepsilon_{p,m},d}_{\varepsilon_{q,m-1},f}\left[\widehat{\rho}(0)\right]^{\varepsilon_{q,m-1},f}_{\varepsilon_{p,m},d}e^{i\omega^{m}_{p,q}n\Delta t}\right)\\ &\quad + h.c., \qquad \text{(A2)}\end{aligned}$$

where "*h.c.*" denotes the Hermitian conjugate, $\mathrm{FID}(k\Delta t)$ can be related to the Fourier coefficients of $g(\omega)$ in Eq. (A2) by

$$\begin{aligned}\mathrm{FID}(k\Delta t) &= \sum_{|\varepsilon_{p,m},d\rangle}\sum_{|\varepsilon_{q,m-1},f\rangle}\left[\widehat{I}_+\right]^{\varepsilon_{p,m},d}_{\varepsilon_{q,m-1},f}\left[\widehat{\rho}(0)\right]^{\varepsilon_{q,m-1},f}_{\varepsilon_{p,m},d}e^{i\omega^{m}_{p,q}k\Delta t}\\ &= (1 + \delta_{k0})\frac{\pi}{\Delta t}(A_k + iB_k). \qquad \text{(A3)}\end{aligned}$$

Under delayed-acquisition for a time $T_{\mathrm{Delay}} = N\Delta t$ for positive integer N, $\mathrm{FID}_{\mathrm{Delay}}(k\Delta t)$ for $k = 0$ to $k = N'_{pts} - 1 = N_{pts} - N - 1$ can be written as

$$\begin{aligned}\mathrm{FID}_{\mathrm{Delay}}(k\Delta t) &= \sum_{|\varepsilon_{p,m},d\rangle}\sum_{|\varepsilon_{q,m-1},f\rangle}\left[\widehat{I}_+\right]^{\varepsilon_{p,m},d}_{\varepsilon_{q,m-1},f}\left[\widehat{\rho}(0)\right]^{\varepsilon_{q,m-1},f}_{\varepsilon_{p,m},d}\\ &\quad \times e^{i\omega^{m}_{p,q}(k+N)\Delta t}\\ &= \frac{\pi}{\Delta t}(A_{N+k} + iB_{N+k}). \qquad \text{(A4)}\end{aligned}$$

Removing the first N Fourier coefficients and shifting higher-order Fourier coefficients to be associated with lower frequency modes has been shown to highlight sharp features in the NMR spectrum.[15] As illustrated in Figs. 4, 5, 7, 9, 10, and 12, delayed-acquisition highlights the "dip" and/or "peak" near $\nu \approx 0$ Hz generated by low-power RF excitation in dipolar solids.

APPENDIX B: MATHEMATICAL PROOFS

1. Proof that diagonal elements of $\widetilde{V}$ in Eq. (14) are less than or equal to 1

Let $\widehat{A}$ be a Hermitian matrix with a set of orthonormal eigenvectors, $|a_n\rangle$ with $\widehat{A}|a_n\rangle = a_n|a_n\rangle$ and $\langle a_m|\widehat{A}|a_n\rangle = a_n\langle a_m|a_n\rangle = a_n\delta_{m,n}$. Since $\widehat{A}$ is hermitian, $\left\langle a_n\middle|\widehat{1} + \left(\widehat{A}\right)^2\middle|a_n\right\rangle = 1 + a_n^2 \geq 1$ (with equality only if $a_n = 0$).

Similarly, for the operator $\widetilde{V} = \frac{\widehat{1}}{\sqrt{\widehat{1}+\left(\widehat{A}\right)^2}}$, $\langle a_n|\widetilde{V}|a_m\rangle = \frac{\delta_{m,n}}{\sqrt{1+a_n^2}} \leq 1$. Thus in the eigenbasis of $\widehat{A}$, the diagonal elements of $\widetilde{V}$ are all less than or equal to 1.

Consider now the diagonal elements of $\widetilde{V}$ in an arbitrary orthonormal basis $|k\rangle$. In that case, we have

$$\begin{aligned}\left[\widetilde{V}\right]_k^k &\equiv \langle k|\widetilde{V}|k\rangle = \sum_{|a_n\rangle}\sum_{|a_m\rangle}\langle k|a_m\rangle\langle a_m|\widetilde{V}|a_n\rangle\langle a_n|k\rangle \\ &= \sum_{|a_n\rangle}\sum_{|a_m\rangle}\frac{\delta_{m,n}}{\sqrt{1+a_n^2}}\langle k|a_m\rangle\langle a_n|k\rangle \\ &= \sum_{|a_n\rangle}\frac{1}{\sqrt{1+a_n^2}}|\langle a_n|k\rangle|^2 \leq \sum_{|a_n\rangle}|\langle a_n|k\rangle|^2 = \langle k|k\rangle = 1,\end{aligned} \tag{B1}$$

and thus $\left[\widetilde{V}\right]_k^k \leq 1$. For $\widehat{A} = \frac{T_p\overline{\overline{\widetilde{H}}}^{(1)}_{\text{AVG}}(T_p)}{\hbar}$ [with $\overline{\overline{\widetilde{H}}}^{(1)}_{\text{AVG}}(T_p)$ given in Eq. (9)], Eq. (B1) indicates that the diagonal elements of $\widetilde{V}$ in Eq. (14) are always less than or equal to 1, i.e., $\left[\widetilde{V}\right]_{\varepsilon_{k,m},d}^{\varepsilon_{k,m},d} \leq 1$.

2. Simultaneous diagonalization of two or more commuting matrices

For two Hermitian matrices $\widehat{A}$ and $\widehat{B}$ with $[\widehat{A}, \widehat{B}] = \widehat{A}\widehat{B} - \widehat{B}\widehat{A} = 0$ (e.g., $\widehat{I}_Z$ and $\widehat{H}_D$), there exists a simultaneous, orthonormal eigenbasis in which both $\widehat{A}$ and $\widehat{B}$ are diagonal. One general procedure for finding such a basis is the diagonalize-one-then-diagonalize-the-other (DODO) approach.[28] In the DODO approach, $\widehat{A}$ is diagonalized to find its orthonormal eigenbasis, $\{|a_k, f\rangle\}$, where $\langle a_j, g|\widehat{A}|a_k, f\rangle = a_k\delta_{kj}\delta_{fg}$. In the $\{|a_k, f\rangle\}$ basis, a condition imposed on the matrix elements of $\widehat{B}$ can be found using $\left[\widehat{A}, \widehat{B}\right] = 0$,

$$\langle a_k, f|\widehat{A}\widehat{B} - \widehat{B}\widehat{A}|a_j, g\rangle = \left(a_k - a_j\right)\langle a_k, f|\widehat{B}|a_j, g\rangle = 0. \tag{B2}$$

In Eq. (B2), $\langle a_k, f|\widehat{B}|a_j, g\rangle = 0$ if $a_k \neq a_j$. However, if there are degeneracies in the spectrum of $\widehat{A}$, i.e., $a_k = a_j$ for $f \neq g$, then $\langle a_k, f|\widehat{B}|a_k, g\rangle$ need not be zero from Eq. (B2). In the $\{|a_k, f\rangle\}$ basis, $\widehat{B}$ is therefore block-diagonal, with the size of the individual blocks determined by the degeneracy of the corresponding eigenvalue of $\widehat{A}$. A second diagonalization of the individual blocks in $\widehat{B}$ is required to provide a simultaneous, orthonormal eigenbasis for both $\widehat{A}$ and $\widehat{B}$.

Below we will prove that if we construct a new matrix $\widehat{C} = \widehat{A} + \lambda\widehat{B}$, where λ is a random, nonzero, real number, the basis $\{|c_k, d_k\rangle\}$, which is found by diagonalizing $\widehat{C}$ with $\langle c_j, d_j|\widehat{C}|c_k, d_k\rangle = c_k\delta_{kj}\delta_{d_j,d_k}$, will, in general, diagonalize both $\widehat{A}$ and $\widehat{B}$. The index $d_k \neq 1$ denotes the degeneracy of states with eigenvalue c_k. If the spectrum of $\widehat{C}$ is non-degenerate (i.e., $d_k = 1$ for all $k = 1$ to N), then the basis $\{|c_k, 1\rangle\}$ forms a simultaneous orthonormal eigenbasis of both $\widehat{B}$ and $\widehat{A}$.

In the following, we will show that in $\{|c_k, d_k\rangle\}$, $\widehat{A}$ and $\widehat{B}$ are diagonal, independent of whether the spectrum of $\widehat{C}$ contains degeneracies or not. Since $\widehat{C} = \widehat{A} + \lambda\widehat{B}$, we can think of the states $\{|c_k, d_k\rangle\}$, and the matrix elements of $\widehat{C}$, $\left[\widehat{C}\right]_{c_k,d_k}^{c_j,f_j} = \langle c_j, f_j|\widehat{C}|c_k, d_k\rangle$, as being parameterized by λ. Following steps similar to those used in the proof of the Hellmann-Feynman theorem,[29] the derivative of $\left[\widehat{C}\right]_{c_k,d_k}^{c_j,f_j} = c_k\delta_{kj}\delta_{d_j,d_k}$ with respect to λ gives

$$\begin{aligned}\frac{\partial}{\partial\lambda}\left(\langle c_j, f_j|\widehat{C}|c_k, d_k\rangle\right) &= \left\langle\frac{\partial c_j, f_j}{\partial\lambda}\middle|\widehat{C}\middle|c_k, d_k\right\rangle + \left\langle c_j, f_j\middle|\widehat{C}\middle|\frac{\partial c_k, d_k}{\partial\lambda}\right\rangle \\ &\quad + \left\langle c_j, f_j\middle|\frac{\partial\widehat{C}}{\partial\lambda}\middle|c_k, d_k\right\rangle \\ &= \left(c_k - c_j\right)\left\langle\frac{\partial c_j, f_j}{\partial\lambda}\middle|c_k, d_k\right\rangle \\ &\quad + \left\langle c_j, f_j\middle|\widehat{B}\middle|c_k, d_k\right\rangle = \frac{\partial c_k}{\partial\lambda}\delta_{kj}\delta_{d_j,d_k},\end{aligned} \tag{B3}$$

where we used the fact that since $\langle c_j, f_j|c_k, d_k\rangle = \delta_{jk}\delta_{f_j,d_k}$,

$$\frac{\partial}{\partial\lambda}\left(\langle c_j, f_j|c_k, d_k\rangle\right) = \left\langle\frac{\partial c_j, f_j}{\partial\lambda}\middle|c_k, d_k\right\rangle + \left\langle c_j, f_j\middle|\frac{\partial c_k, d_k}{\partial\lambda}\right\rangle = 0. \tag{B4}$$

From Eq. (B3), if $c_j = c_k$ and $d_k \neq f_k$, then $\langle c_k, f_k|\widehat{B}|c_k, d_k\rangle = 0$. If $c_j \neq c_k$, then $\langle c_j, f_j|\widehat{B}|c_k, d_k\rangle = 0$ from Eq. (B2) since $\left[\widehat{C}, \widehat{B}\right] = 0$. Thus $\widehat{B}$ is diagonal in the $\{|c_k, d_k\rangle\}$ basis. Furthermore, since the off-diagonal elements of $\widehat{C}$ in the basis $\{|c_k, d_k\rangle\}$ are also zero, i.e., $\langle c_j, f_j|\widehat{C}|c_k, d_k\rangle = 0$ when $c_j \neq c_k$ and/or $f_j \neq d_k$, then

$$\begin{aligned}\langle c_j, f_j|\widehat{C}|c_k, d_k\rangle &= \langle c_j, f_j|\widehat{A}|c_k, d_k\rangle + \lambda\langle c_j, f_j|\widehat{B}|c_k, d_k\rangle \\ &= \langle c_j, f_j|\widehat{A}|c_k, d_k\rangle = 0.\end{aligned} \tag{B5}$$

Therefore $\widehat{A}$ is also diagonal in the basis $\{|c_k, d_k\rangle\}$. Thus an orthonormal eigenbasis found by diagonalizing $\widehat{C} = \widehat{A} + \lambda\widehat{B}$ for nonzero and real λ also forms an orthonormal eigenbasis for both $\widehat{A}$ and $\widehat{B}$.

It should be noted that one important condition for the above proof is that the rank of matrix $\widehat{C}$ must be equal to the maximum rank of either $\widehat{A}$ or $\widehat{B}$. As an extreme example, suppose $\widehat{B} = -\widehat{A} \neq \widehat{0}$ and $\lambda = 1$. In that case, $\widehat{C} = \widehat{A} + \lambda\widehat{B} = \widehat{0}$, and the above proof would not be valid. If λ is randomly chosen, the likelihood of the rank of $\widehat{C}$ being reduced relative to either $\widehat{A}$ and/or $\widehat{B}$ is negligible. Note that the above proof can also be expanded to the case of three or more commuting matrices.

[1] N. Bloembergen, E. Purcell, and R. V. Pound, "Relaxation effects in nuclear magnetic resonance absorption," Phys. Rev. **73**, 679–712 (1948).

[2] G. A. Morris and R. Freeman, "Selective excitation in Fourier-transform nuclear magnetic resonance," J. Magn. Reson. **29**, 433–462 (1978).

[3] E. E. Sigmund and W. P. Halperin, "Hole-burning diffusion measurements in high magnetic field gradients," J. Magn. Reson. **163**, 99–104 (2003).

[4] M. Todica and B. Blumich, "Hole-burning NMR in strongly inhomogeneous fields," Sol. Stat. Nucl. Magn. Reson. **32**, 66–70 (2007).

[5] B. N. Provotorov, "Magnetic resonance saturation in crystals," Sov. Phys. JETP **14**, 1126–1131 (1962).

[6] M. Goldman, *Spin Temperature and Nuclear Magnetic Resonance in Solids* (Oxford University Press, London, 1970).

[7] A. K. Khitrin, V. L. Ermakov, and B. M. Fung, "Nuclear magnetic resonance molecular photography," J. Chem. Phys. **117**, 6903–6906 (2002).

[8] B. M. Fung and V. L. Ermakov, "Selective excitation in spin systems with homogeneous broadening," J. Chem. Phys. **120**, 9624 (2004).

[9] A. K. Khitrin, "Long-lived NMR echoes in solids," J. Magn. Reson. **213**, 22–25 (2011).

[10] A. K. Khitrin, "Selective excitation of homogeneous spectral lines," J. Chem. Phys. **134**, 154502 (2011).

[11] B. Y. Zhang, J. S. Lee, A. Khitrin, and A. Jerschow, "Long lived NMR signal in bone," J. Magn. Reson. **231**, 1–4 (2013).

[12] M. Alla and E. Lippmaa, "Resolution limits in magic-angle rotation NMR spectra of polycrystalline solids," Chem. Phys. Lett. **87**, 30–33 (1982).

[13] U. Schwerk, D. Michel, and M. Pruski, "Local magnetic field distribution in a polycrystalline sample exposed to a strong magnetic field," J. Magn. Reson., Ser. A **119**, 157–164 (1996).

[14] Z. Gong and J. D. Walls, "Breakdown of linear response theory under low-power excitation in NMR. I. The case of long-lived signals in inhomogeneously broadened spin systems," J. Chem. Phys. **145**, 164201 (2016).

[15] Z. Gong and J. D. Walls, "Enhancing the detection of edges and non-differentiable points in an NMR spectrum using delayed-acquisition," J. Magn. Reson. **287**, 15–24 (2018).

[16] U. Haeberlen and J. S. Waugh, "Coherent averaging effects in magnetic resonance," Phys. Rev. **175**, 453–467 (1968).

[17] P. W. Langhoff, S. T. Epstein, and M. Karplus, "Aspects of time-dependent perturbation theory," Rev. Mod. Phys. **44**, 602–644 (1972).

[18] J. D. Walls and Y. Y. Lin, "Constants of motion in NMR spectroscopy," Solid State Nucl. Magn. Reson. **29**, 22–29 (2006).

[19] See http://www.mathworks.com for Mathworks, Matlab.

[20] J. J. Helmus and C. P. Jaroniec, "Nmrglue: An open source Python package for the analysis of multidimensional NMR data," J. Biomol. NMR **55**, 355–367 (2013).

[21] A. Schenzle, N. C. Wong, and R. G. Brewer, "Theorem on coherent transients," Phys. Rev. A **22**, 635–637 (1980).

[22] A. G. Anderson, R. L. Garwin, E. L. Hahn, J. W. Horton, G. L. Tucker, and R. M. Walker, "Spin echo serial storage memory," J. Appl. Phys. **26**, 1324–1338 (1955).

[23] C. D. Ridge, L. F. O'Donnell, and J. D. Walls, "Long-lived selective spin echoes in dipolar solids under periodic and aperiodic π-pulse trains," Phys. Rev. B **89**, 024404 (2014).

[24] H. W. Spiess, H. Zimmermann, and U. Haeberlen, "Proton magnetic shielding and susceptibility effects in single crystals of ferrocene," Chem. Phys. **12**, 123–130 (1976).

[25] K. Lonsdale, "The structure of the benzene ring," Nature **122**, 810 (1928).

[26] E. R. Andrew, "Molecular motion in certain solid hydrocarbons," J. Chem. Phys. **18**, 607–618 (1950).

[27] M. A. Frey, M. Michaud, J. N. VanHouten, K. L. Insogna, J. A. Madri, and S. E. Barrett, "Phosphorus-31 MRI of hard and soft solids using quadratic echo line-narrowing," Proc. Nat. Acad. Sci. U. S. A. **109**, 5190–5195 (2012).

[28] A. Bunse-Gerstner, R. Byers, and V. Mehrmann, "Numerical methods for simultaneous diagonalization," SIAM J. Matrix Anal. Appl. **14**, 927–949 (1993).

[29] R. P. Feynman, "Forces in molecules," Phys. Rev. **56**, 340–343 (1939).

Supporting Information: Breakdown of linear response theory under low-power excitation in NMR. II: The case of "long-lived" signals in homogeneously broadened dipolar spin systems.

Zhaoyuan Gong[1] and Jamie D. Walls[1]

[1]*Department of Chemistry, University of Miami, Coral Gables, Florida 33124,USA*

(Dated: November 1, 2018)

Abstract

Additional details about the numerical simulations of a linear spin chain, the nature of $\widetilde{V}$ in the unitarity-corrected LR propagator, the connection between ω_{RF} and $\text{FID}_{LPP}^{\pi,LR}(t)$, experiments in hexamethylbenzene, and pulse programs are provided.

I. NATURE OF $\widetilde{V}$ IN THE UNITARY-CORRECTED LR PROPAGATOR

The operator $\widetilde{V}$ in Eq. (14) of the main text was introduced to enforce the unitarity of the LR propagator. As previously mentioned, $\widetilde{V}$ will contain both diagonal and off-diagonal elements due to the interconnectedness of the eigenstates of $\widehat{H}_0 = \widehat{H}_D + \widehat{H}_{cs} + \widehat{H}_{\text{offset}}$ under RF excitation. As given in Eq. (14) of the main text,

$$\begin{aligned}\widetilde{V} &= \left(\widehat{1} + \left(\frac{T_p \overline{\overline{\widetilde{H}}}{}^{(1)}_{\mathrm{AVG}}(T_p)}{\hbar}\right)^2\right)^{-\frac{1}{2}} = \sum_{k=0}^{\infty} (-1)^k \frac{(2k-1)!!}{(2k)!!} \left(\frac{T_p \overline{\overline{\widetilde{H}}}{}^{(1)}_{\mathrm{AVG}}(T_p)}{\hbar}\right)^{2k} \\ &\approx \widehat{1} - \frac{1}{2}\left(\frac{T_p \overline{\overline{\widetilde{H}}}{}^{(1)}_{\mathrm{AVG}}(T_p)}{\hbar}\right)^2 \end{aligned} \tag{1}$$

where $a!!$ is a double factorial. In the last line of Eq. (1), $\widetilde{V}$ was approximated by the first two terms of the Taylor series since we were interested in examining the lowest-order contributions of the RF to $\widetilde{V}$ (such an approximation is also generally valid when $\omega_{RF} T_p \equiv \Theta < 1$). $\widetilde{V}$ in Eq. (1) can be rewritten in terms of its diagonal $\left(\widetilde{V}_{\text{diag}}\right)$ and off-diagonal $\left(\widetilde{V}_{\text{off-diag.}}\right)$ elements, the latter of which contains both $\left(\widetilde{V}_{0Q}\right)$ zero- and $\left(\widetilde{V}_{2Q}\right)$ double-quantum transitions:

$$\begin{aligned}\widetilde{V} &\approx \widehat{1} - \frac{1}{2}\left(\frac{T_p \overline{\overline{\widetilde{H}}}{}^{(1)}_{\mathrm{AVG}}(T_p)}{\hbar}\right)^2 \equiv \widetilde{V}_{\text{diag}} + \widetilde{V}_{\text{off-diag.}} \\ \widetilde{V}_{\text{off-diag.}} &= \widetilde{V}_{0Q} + \widetilde{V}_{2Q}\end{aligned} \tag{2}$$

In the eigenbasis of $\widehat{H}_0$, $\left\{|\varepsilon_{k,m}, d\rangle\right\}$, the diagonal matrix elements of $\widetilde{V}$, $\left[\widetilde{V}\right]^{\varepsilon_{k,m},d}_{\varepsilon_{k,m},d} \equiv \langle \varepsilon_{k,m}, d|\widetilde{V}|\varepsilon_{k,m}, d\rangle$, are given for a constant, low-power pulse applied for a time T_p by:

$$\left[\widetilde{V}\right]^{\varepsilon_{k,m},d}_{\varepsilon_{k,m},d} \approx 1 - \frac{\Theta^2}{4} \sum_{|\varepsilon_{j,m\pm1},f\rangle} \operatorname{sinc}^2\left(\frac{\Delta\omega \mp \omega^{m,m\pm1}_{k,j}}{2\omega_{RF}}\Theta\right) \left|\left[\widehat{I}_{\mp}\right]^{\varepsilon_{k,m},d}_{\varepsilon_{j,m\pm1},f}\right|^2 \tag{3}$$

where $\Theta = \omega_{RF} T_p$. From Eq. (3), the diagonal elements are all less than 1 which is consistent with the exact results given in Appendix B of the main text.

The zero-quantum matrix elements of $\widetilde{V}$, $\left[\widetilde{V}\right]^{\varepsilon_{k,m},d}_{\varepsilon_{l,m},g} \equiv \left[\widetilde{V}_{0Q}\right]^{\varepsilon_{k,m},d}_{\varepsilon_{l,m},g}$ for $|\varepsilon_{k,m}, d\rangle \neq |\varepsilon_{l,m}, g\rangle$, are given by:

$$\left[\widetilde{V}_{0Q}\right]^{\varepsilon_{k,m},d}_{\varepsilon_{l,m},g} \approx -\frac{\Theta^2}{4} \sum_{|\varepsilon_{j,m\pm1},f\rangle} e^{i\omega^{m,m}_{k,l}\frac{T_p}{2}} \operatorname{sinc}\left(\frac{\Delta\omega \mp \omega^{m,m\pm1}_{k,j}}{2\omega_{RF}}\Theta\right) \operatorname{sinc}\left(\frac{\Delta\omega \mp \omega^{m,m\pm1}_{l,j}}{2\omega_{RF}}\Theta\right) \left[\widehat{I}_{\mp}\right]^{\varepsilon_{k,m},d}_{\varepsilon_{j,m\pm1},f} \left[\widehat{I}_{\pm}\right]^{\varepsilon_{j,m\pm1},f}_{\varepsilon_{l,m},g} \tag{4}$$

while the double-quantum matrix elements of $\widetilde{V}$, $\left[\widetilde{V}\right]^{\varepsilon_{j,m\pm1},f}_{\varepsilon_{p,m\mp1},g} \equiv \left[\widetilde{V}_{2Q}\right]^{\varepsilon_{j,m\pm1},f}_{\varepsilon_{p,m\mp1},g}$, are given by:

$$\begin{aligned}\left[\widetilde{V}_{2Q}\right]^{\varepsilon_{j,m\pm1},f}_{\varepsilon_{p,m\mp1},g} \approx \frac{\Theta^2}{4} \sum_{|\varepsilon_{k,m},d\rangle} e^{i(\omega_{j,p}^{m\pm1,m\mp1} \pm 2\Delta\omega)\frac{T_p}{2}} \operatorname{sinc}\left(\frac{\omega_{j,k}^{m\pm1,m} \pm \Delta\omega}{2\omega_{RF}}\Theta\right) \operatorname{sinc}\left(\frac{\omega_{k,p}^{m,m\mp1} \pm \Delta\omega}{2\omega_{RF}}\Theta\right) \\ \times \left[\widehat{I}_{\pm}\right]^{\varepsilon_{j,m\pm1},f}_{\varepsilon_{k,m},d} \left[\widehat{I}_{\pm}\right]^{\varepsilon_{k,m},d}_{\varepsilon_{p,m\mp1},g}\end{aligned} \tag{5}$$

For a state $|\varepsilon_{k,m},d\rangle$, if $|\omega_{k,j}^{m,m\mp1} \mp \Delta\omega| \gg \omega_{RF}$ for all states $|\varepsilon_{j,m\mp1},f\rangle$ that are connected to $|\varepsilon_{k,m},d\rangle$ by the RF, then for $\Theta < 1$, the diagonal elements scale as:

$$\left[\widetilde{V}\right]^{\varepsilon_{k,m},d}_{\varepsilon_{k,m},d} \sim 1 - \sum_{|\varepsilon_{j,m\pm1},f\rangle} \left(\frac{\omega_{RF}}{\left|\Delta\omega \mp \omega_{k,j}^{m,m\pm1}\right|}\right)^2 \left|\left[\widehat{I}_{\mp}\right]^{\varepsilon_{k,m},d}_{\varepsilon_{j,m\pm1},f}\right|^2 \approx 1 \tag{6}$$

where we used the approximation that $\operatorname{sinc}(x) \sim \frac{1}{x}$ for $x \gg 1$. Similarly, the off-diagonal elements under similar conditions scale as:

$$\begin{aligned}\left[\widetilde{V}_{0Q}\right]^{\varepsilon_{k,m},d}_{\varepsilon_{l,m},g} &\sim -\sum_{|\varepsilon_{j,m\pm1},f\rangle} e^{i\omega_{k,l}^{m,m}\frac{T_p}{2}} \frac{\omega_{RF}^2}{\left(\Delta\omega \mp \omega_{k,j}^{m,m\pm1}\right)\left(\Delta\omega \mp \omega_{l,j}^{m,m\pm1}\right)} \left[\widehat{I}_{\mp}\right]^{\varepsilon_{k,m},d}_{\varepsilon_{j,m\pm1},f} \left[\widehat{I}_{\pm}\right]^{\varepsilon_{j,m\pm1},f}_{\varepsilon_{l,m},g} \approx 0 \\ \left[\widetilde{V}_{2Q}\right]^{\varepsilon_{j,m\pm1},f}_{\varepsilon_{p,m\mp1},g} &\sim \sum_{|\varepsilon_{k,m},d\rangle} e^{i(\omega_{j,p}^{m\pm1,m\mp1} \pm 2\Delta\omega)\frac{T_p}{2}} \frac{\omega_{RF}^2}{\left(\omega_{j,k}^{m\pm1,m} \pm \Delta\omega\right)\left(\omega_{k,p}^{m,m\mp1} \pm \Delta\omega\right)} \left[\widehat{I}_{\pm}\right]^{\varepsilon_{j,m\pm1},f}_{\varepsilon_{k,m},d} \left[\widehat{I}_{\pm}\right]^{\varepsilon_{k,m},d}_{\varepsilon_{p,m\mp1},g} \approx 0\end{aligned} \tag{7}$$

Thus for such states that are only weakly coupled by the low-power RF, $\widetilde{V}$ is independent of Θ and behaves like the identity operator for those states. As such, the contribution from weakly coupled states to $\mathrm{FID}_{LPP}(t)$ is similar to that predicted using LR theory in Eq. (11) of the main text.

In contrast, for a state $|\varepsilon_{k,m},d\rangle$ that is strongly coupled by the applied RF, i.e., $|\omega_{k,j}^{m,m\mp1} \mp \Delta\omega| \ll \omega_{RF}$ to all states $|\varepsilon_{j,m\mp1},f\rangle$ that are connected to it by the RF, then for $\Theta < 1$, the diagonal elements scale as:

$$\left[\widetilde{V}\right]^{\varepsilon_{k,m},d}_{\varepsilon_{k,m},d} \sim 1 - \frac{\Theta^2}{4} \sum_{|\varepsilon_{j,m\pm1},f\rangle} \left|\left[\widehat{I}_{\mp}\right]^{\varepsilon_{k,m},d}_{\varepsilon_{j,m\pm1},f}\right|^2 < 1 \tag{8}$$

where we used $\operatorname{sinc}(x) \sim 1$ for $x \ll 1$. Similarly, the off diagonal elements of $\widetilde{V}$ scale as:

$$\begin{aligned}\left[\widetilde{V}_{0Q}\right]^{\varepsilon_{k,m},d}_{\varepsilon_{l,m},g} &\sim -\frac{\Theta^2}{4} \sum_{|\varepsilon_{j,m\pm1},f\rangle} e^{i\omega_{k,l}^{m,m}\frac{T_p}{2}} \left[\widehat{I}_{\mp}\right]^{\varepsilon_{k,m},d}_{\varepsilon_{j,m\pm1},f} \left[\widehat{I}_{\pm}\right]^{\varepsilon_{j,m\pm1},f}_{\varepsilon_{l,m},g} \\ \left[\widetilde{V}_{2Q}\right]^{\varepsilon_{j,m\pm1},f}_{\varepsilon_{p,m\mp1},g} &\sim \frac{\Theta^2}{4} \sum_{|\varepsilon_{k,m},d\rangle} e^{i(\omega_{j,p}^{m\pm1,m\mp1} \pm 2\Delta\omega)} \left[\widehat{I}_{\pm}\right]^{\varepsilon_{j,m\pm1},f}_{\varepsilon_{k,m},d} \left[\widehat{I}_{\pm}\right]^{\varepsilon_{k,m},d}_{\varepsilon_{p,m\mp1},g}\end{aligned} \tag{9}$$

In this case, the diagonal elements of $\widetilde{V}$ attenuate the contributions to the FID after low-power excitation from those states where the RF represents a strong perturbation. The off-diagonal elements in Eq. (9) scale as Θ^2 and consist of sums over complex terms that need not constructively add together, thereby reducing the magnitude of the off-diagonal matrix elements (this is in contrast to the terms in the summand for the diagonal elements in Eq. (8) which are always positive.). Due to the Θ scaling, neglecting spectra diffusion appears to be generally justified in the LR regime $(\Theta \leq \frac{\pi}{3}$.

From the numerical simulations on an $N_s = 10$ linear spin chain show in Fig. 3, making the approximation $\widetilde{V} \approx \widetilde{V}_{\text{diag.}}$ (i.e., neglecting spectral diffusion during the pulse) appears to be justified for $\Theta \leq \pi$. To get a more semi-quantitative understanding when neglecting spectral diffusion during the pulse is justified, numerical calculations of the relative contribution of $\widetilde{V}_{\text{off-diag.}}$ to $\widetilde{V}$, $\frac{||\widetilde{V}_{\text{off-diag.}}||}{||\widetilde{V}||}$, were performed, where $||\widehat{A}|| = \sqrt{\text{Tr}\left[\widehat{A}^{\dagger}\widehat{A}\right]}$ represents the Frobenius norm of the matrix $\widehat{A}$. In Fig. 1, $\frac{||\widetilde{V}_{\text{off-diag.}}||}{||\widetilde{V}||}$ as a function of $\Theta = 2\pi\nu_{RF}T_p$ is plotted under conditions of either (A) fixed $\nu_{RF} = 1$ Hz or (C) fixed $T_p = 250$ ms. The red line represents the mean value of $\frac{||\widetilde{V}_{\text{off-diag.}}||}{||\widetilde{V}||}$ averaged over $N_{\text{AVG}} = 160$ different spatial configurations of the linear spin chain (details are given in Fig. 1), with the blue error bars representing ± a standard deviation. As can be seen in Fig. 1, the contributions of the off-diagonal terms to $\widetilde{V}$ for $\Theta \leq \pi$ is (C) less than 5% for fixed T_p and (A) less than 10% for fixed ν_{RF}. For the linear spin chain, neglect of spectral diffusion during the RF pulse therefore appears to be a good approximation when $\Theta \leq \pi$, which is consistent with the simulations shown in Fig. 3. Additionally, the average diagonal elements, $\left[\widetilde{V}\right]_{\varepsilon_{k,m},d}^{\varepsilon_{k,m},d} \equiv \left[\widetilde{V}\right]_k^k$ were also calculated for $k = 1$ to $k = 2^{10} = 1024$. In this case, the states were first arranged in order of increasing $\varepsilon_{k,m}$ from negative to positive values before averaging $\left[\widetilde{V}\right]_k^k$ for a given k. In all cases, $\left[\widetilde{V}\right]_k^k$ tended to decrease as Θ increased. Furthermore, larger values of ν_{RF} tended to lead to smaller $\left[\widetilde{V}\right]_k^k$ even for the same $\Theta = 2\pi\nu_{RF}T_p$ [Figs. 1(B) vs. 1(D)].

II. NUMERICAL SIMULATIONS ON AN $N_s = 10$ LINEAR SPIN $I = \frac{1}{2}$ CHAIN

In Fig. 2, numerical simulations were performed on an $N_s = 10$ linear spin chain oriented along the $\widehat{z}$-direction (details of the simulation are given in the main text) with $\Delta\omega = 0$, i.e., only pure dipolar evolution was considered. Low-power excitation by a constant pulse shape $(\omega_{RF}(t) = 2\pi\nu_{RF}\,\text{for}\,0 \leq t \leq T_p)$ was calculated using either fixed $\nu_{RF} = 1$ Hz [Figs. 2(A) and

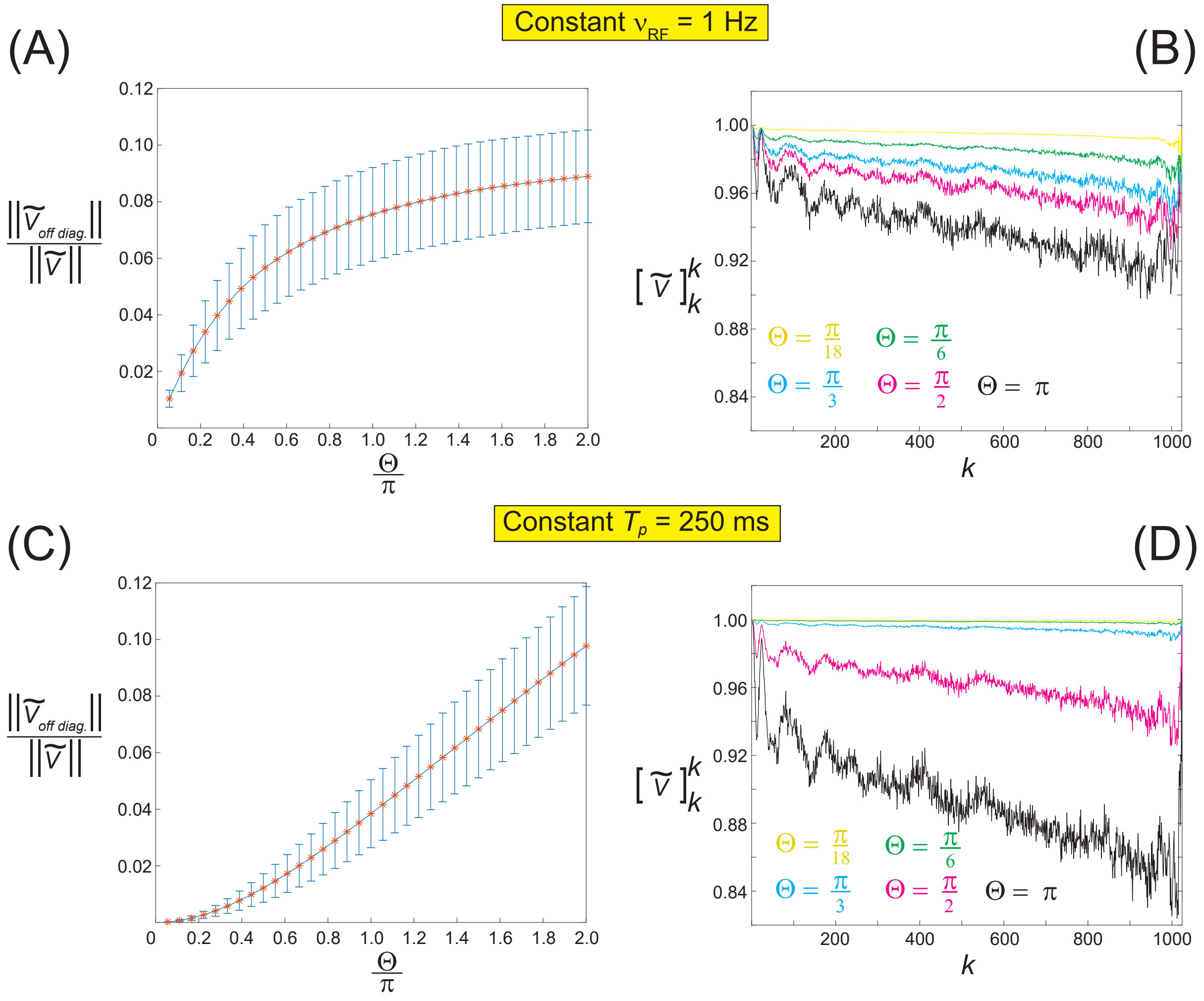

FIG. 1. Calculations of $\widetilde{V} = \widetilde{V}_{\text{diag.}} + \widetilde{V}_{\text{off-diag.}}$ for an $N_s = 10$ linear spin chain ($I = \frac{1}{2}$) under low-power excitation. In these simulations, only evolution under $\widehat{H}_D$ was considered (i.e., $\Delta\omega = 0$), and low-power excitation by a constant pulse shape under conditions of either [(A) and (B)] fixed $\nu_{RF} = 1$ Hz or [(C) and (D)] fixed $T_p = 250$ ms were simulated. All the results in Fig. 2 represent an average over $N_{\text{AVG}} = 160$ different spatial configurations similar to those used in Fig. 2 of the main text. In this case, the average distance of the k^{th} spin was given by $\overline{|\vec{r}_k|} = (k-1)d \pm \delta r$ where $\delta r \approx 0.06d$ with $\frac{\gamma^2\hbar}{2\pi d^3} = 35$ Hz. In (A) and (C), the average size of $\widetilde{V}_{\text{off-diag.}}$ relative to $\widetilde{V}$, $\frac{||\widetilde{V}_{\text{off-diag.}}||}{||\widetilde{V}||}$, as a function of $\Theta = 2\pi\nu_{RF}T_p$ was calculated with the red line showing the average value of $\frac{||\widetilde{V}_{\text{off-diag.}}||}{||\widetilde{V}||}$, with the blue error bars representing ± one standard deviation ($||\widehat{A}|| = \sqrt{\text{Tr}\left[\widehat{A}^{\dagger}\widehat{A}\right]}$ represents the Frobenius norm of $\widehat{A}$). For $\Theta \leq \pi$, the off-diagonal elements make up less than (C) 5% of $\widetilde{V}$ for constant T_p and less than (A) 10% for fixed ν_{RF}. In (B) and (D), the average value of the diagonal elements of $\widetilde{V}$, $\left[\widetilde{V}\right]_{\varepsilon_k,d}^{\varepsilon_k,d} \equiv \left[\widetilde{V}\right]_k^k$ for $k = 1$ to $k = 1024$ is plotted for different nominal $\Theta = 2\pi\nu_{RF}T_p$ (see the text for details). In all cases, the diagonal elements were always less than 1 and decreased in magnitude with increasing Θ.

2(C)] or fixed $T_p = 250$ ms [Figs. 2(B) and 2(D)]. The spectra represent an average over either $N_{\text{AVG}} = 200$ different $\vec{r}_{\text{spins}}$ [Figs. 2(A) and 2(B), which were the same $\vec{r}_{\text{spins}}$ used in Figure 2 in the main text] or $N_{\text{AVG}} = 2000$ $\vec{r}_{\text{spins}}$ [Figs. 2(C) and 2(D)]. For fixed time ($T_p = 250$ ms), the spectra were nearly identical for both $N_{\text{AVG}} = 200$ and $N_{\text{AVG}} = 2000$ [Fig. 2(B) vs. Fig. 2(D)]. Furthermore, the intensity at $\nu \approx 0$ Hz decreased with increasing Θ. For $\Theta \leq \frac{\pi}{3}$, the dispersive signal for $\left|\nu_{k,j}^{m,m-1}\right| > 0$ Hz was apparently not enough to dominate the positive contributions from transition frequencies $\left|\nu_{k,j}^{m,m-1}\right| \approx 0$ Hz (as illustrated in Figure 1 in the main text). As a result, the low-power spectra contained a peak near $\nu \approx 0$ Hz that did get smaller with increasing $\Theta \leq \frac{\pi}{3}$; for $\Theta = \frac{\pi}{2}$ and $\Theta = \pi$, only a negative "dip" was observed near $\nu \approx 0$ Hz.

For constant $\nu_{RF} = 1$ Hz, there were slight differences in the low-power excitation spectra between averaging [Fig. 2(A)] $N_{\text{AVG}} = 200$ and [Fig. 2(C)] $N_{\text{AVG}} = 2000$ different $\vec{r}_{\text{spins}}$. In particular, there was more positive signal near $\nu \approx 0$ Hz when averaging over fewer $\vec{r}_{\text{spins}}$ for $\Theta \leq \frac{\pi}{3}$ [Fig. 2(A) vs. Fig. 2(C)]. However, a negative "dip" near $\nu \approx 0$ Hz was observed for $\Theta = \frac{\pi}{2}$ and $\Theta = \pi$ in both cases [Figs. 2(A) and 2(C)].

In Figure 3, the effects of making the approximation $\widetilde{V} \approx \widetilde{V}_{\text{diag.}}$ (i.e., neglecting spectral diffusion during the RF pulse) on the low-power excitation spectra in a linear spin chain are presented. In this case, identical calculations to those presented in Figure 2 of the main text are shown using unitarity-corrected linear response theory with either the (green) exact $\widetilde{V}$ or by making the approximation (black) $\widetilde{V} \approx \widetilde{V}_{\text{diag.}}$. For comparison, the linear response spectra [red, which were also shown in Fig. 2 of the main text] are also plotted. Overall, the calculated spectra using either the (green) exact $\widetilde{V}$ or (black) $\widetilde{V} \approx \widetilde{V}_{\text{diag.}}$ were very similar, with only minor differences near $\nu \approx 0$ Hz. These simulations indicate that the "homogeneous" broadening terms, i.e., the off-diagonal terms of $\widetilde{V}$, can be safely neglected for low-power excitation with $\Theta \leq \pi$ in a linear spin chain.

III. DEPENDENCE OF $\text{FID}^{\pi}_{LPP}(t)$ ON $\omega_{RF}(t)$

Consider an inhomogeneously broadened system with a frequency distribution, $g(\omega)$. The FID after a $\frac{\pi}{2}$Y-pulse can be written as:

$$\text{FID}_{\frac{\pi}{2}Y}(t) = \frac{1}{2}\int d\omega g(\omega) e^{i\omega t} \tag{10}$$

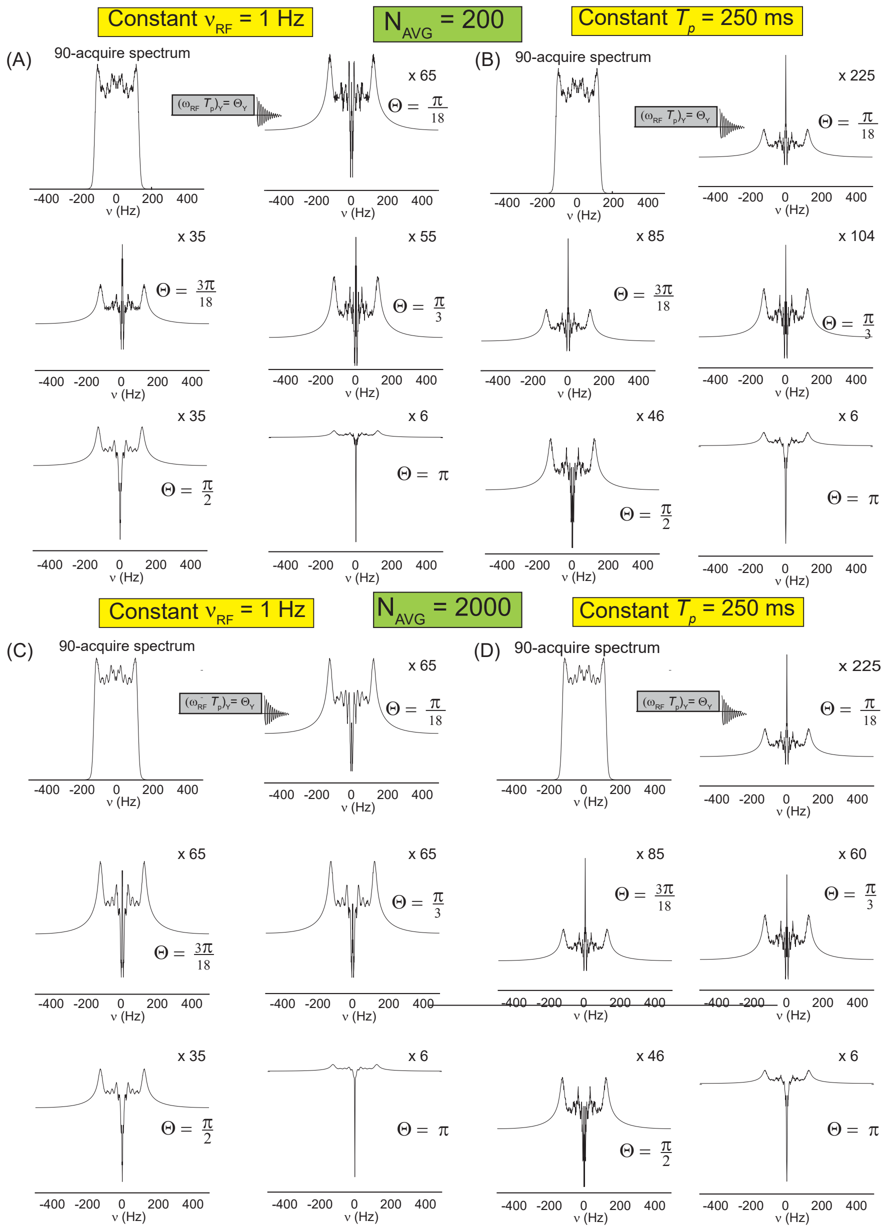

FIG. 2. Numerical simulations ($N_{pts} = 1000$ and $\Delta t = 1$ ms) for an $N_s = 10$ linear spin chain ($I = \frac{1}{2}$) under low-power excitation. In these simulations, only evolution under $\widehat{H}_D$ was considered (i.e., $\Delta\omega = 0$), and low-power excitation by a constant, RF pulse shape under conditions of either constant $\nu_{RF} = 1$ Hz or fixed $T_p = 250$ ms was simulated. In (A) and (B), the results were averaged over the same $N_{\mathrm{AVG}} = 200$ spatial configurations used in Fig. 2 of the main text (in this case, the average distance of the k^{th} spin was given by $\overline{|\vec{r}_k|} = (k-1)d \pm \delta r$ where $\delta r \approx 0.06d$ with $\frac{\gamma^2\hbar}{2\pi d^3} = 35$ Hz). In (C) and (D), the results were averaged over $N_{\mathrm{AVG}} = 2000$ different $\vec{r}_{\mathrm{spins}}$ (in this case, the average distance of the k^{th} spin was also given by $\overline{|\vec{r}_k|} = (k-1)d \pm \delta r$ where $\delta r \approx 0.06d$).

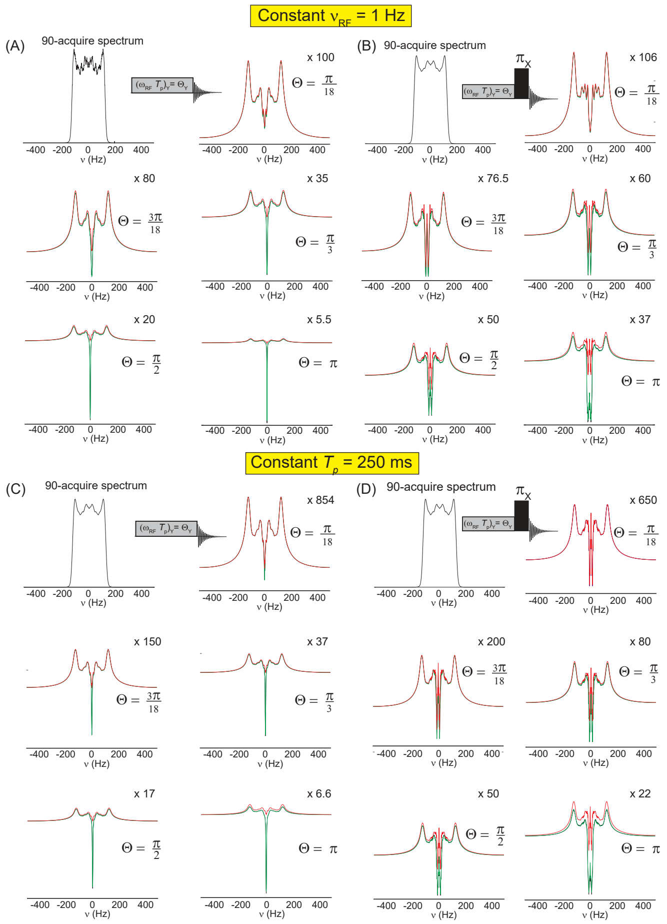

FIG. 3. Numerical simulations of the spectra under $\widehat{H}_0 = \widehat{H}_D + \hbar\Delta\omega\widehat{I}_Z$ derived from low-power excitation by a constant RF pulse shape, with and without application of a π_X-pulse, in an $N_s = 10$ linear spin chain and averaged over $N_{\text{AVG}} = 200$ spatial configurations (the same as used in Figs. 2(A) and 2(B) and also used in Fig. 2 of the main text). For each $\vec{r}_{\text{spins}}$, the evolution for 41 different values of $\Delta\omega$ uniformly distributed over the range $\frac{\Delta\omega}{2\pi} \in [-10\,\text{Hz}, 10\,\text{Hz}]$ were averaged for $\Theta = 2\pi\nu_{RF}T_p \in \left\{\frac{\pi}{18}, \frac{\pi}{6}, \frac{\pi}{3}, \frac{\pi}{2}, \pi\right\}$ under conditions of either constant ν_{RF} [$\nu_{RF} = 1$ Hz in Fig. 3(A) and 3(B)] or constant T_p [$T_p = 250$ ms in Fig. 3(C) and 3(D)]. The linear response spectra [Eq. (7) in the main text, red] and the unitarity-corrected linear response spectra using either the (green) exact $\widetilde{V}$ or by making the approximation (black) $\widetilde{V} \approx \widetilde{V}_{\text{diag.}}$ are presented. The spectra calculated using the approximation $\widetilde{V} \approx \widetilde{V}_{\text{diag.}}$ (black) were not noticeably different from those using the exact $\widetilde{V}$ (green), suggesting that "homogeneous" broadening during the RF pulse did not significantly affect the spectrum for $\Theta \leq \pi$ in the linear spin chain simulations.

The FID after low-power excitation by an RF pulse (in the LR regime) of length T_p and shape $\omega_{RF}(t)$ followed by a π_X-pulse, $\mathrm{FID}^{\pi,LR}_{LPP}(t)$, is given by[1]:

$$\begin{aligned}\mathrm{FID}^{\pi,LR}_{LPP}(t) &= \int_{-\infty}^{\infty} dt'\,\omega_{RF}(t')\mathrm{FID}_{\frac{\pi}{2}Y}(t-T_p+t') \\ &\equiv \omega_{RF}\star\mathrm{FID}_{\frac{\pi}{2}Y}(t-T_p)\end{aligned} \tag{11}$$

where the limits of integration were extended to ±∞ since $\omega_{RF}(t)=0$ for $t>T_p$ and $t<0$. From Eq. (11), the signal is given by the cross-correlation of $\omega_{RF}(t)$ with the $\mathrm{FID}_{\frac{\pi}{2}Y}(t-T_p)$. Note that for $0\le t\le T_p$, the argument of $\mathrm{FID}_{\frac{\pi}{2}Y}(t'+t-T_p)$ in the integrand in Eq. (11) can be negative even though the FID in Eq. (10) is technically only defined for times after the pulse ($t>0$). This is a result of the π_X-pulse reversing the sign of the frequency evolution in Eq. (10), thereby making the system appear to evolve effectively with a negative time. Therefore, whenever $t-T_p+t'\le 0$, $\mathrm{FID}_{\frac{\pi}{2}Y}(t-T_p+t')=\left(\mathrm{FID}_{\frac{\pi}{2}Y}(|t-T_p+t'|)\right)^*$ in the integrand of Eq. (11).

One consequence of $\mathrm{FID}^{\pi,LR}_{LPP}(t)$ being the cross-correlation of $\omega_{RF}(t)$ with $\mathrm{FID}_{\frac{\pi}{2}Y}(t-T_p)$ is that $\mathrm{FID}^{\pi,LR}_{LPP}(t)$ resembles the time-reversed RF pulse shape. This is illustrated in Fig. 4 for a ramped pulse shape, $\omega_{RF}(t)=2\Theta\frac{t}{T_p^2}$ for $0\le t\le T_p$ for $T_p=3$ ms and $\Theta=\frac{\pi}{3}$, applied to an inhomogeneously broadened spin-$\frac{1}{2}$ system (the $\mathrm{FID}_{\frac{\pi}{2}Y}(t)$ and the corresponding spectrum $S(\nu)$ are shown in Fig. 4). As can be seen at times $t=0$, $t=0.4$ ms, $t=1.5$ ms, and $t=T_p=3$ ms (which are denoted by '*'), the overlap of $\omega_{RF}(t)$ with the $\mathrm{FID}_{\frac{\pi}{2}Y}(t)$ (denoted by red in Fig. 4) is maximal at early times and decreases as $t\to T_p$. In effect, $\mathrm{FID}_{\frac{\pi}{2}Y}$ "scans" the applied RF from the end of the pulse (corresponding to time $t=0$) to the beginning of the pulse (corresponding to time $t=T_p$), thus making $\mathrm{FID}^{\pi,LR}_{LPP}(t)$ resemble the time-reversed pulse shape.

IV. EFFECTS OF THE SIZE OF THE INHOMOGENEOUS LINEWIDTH, $\Delta\omega_{\frac{1}{2}}$, RELATIVE TO ω_{RF} ON $\mathrm{FID}^{\pi}_{LPP}(t)$ AT $t\approx T_p$ IN AN INHOMOGENEOUSLY BROADENED SPIN SYSTEM

Simulations of $\mathrm{FID}^{\pi}_{LPP}(t)$ were also performed for an inhomogeneously broadened spin ($I=1/2$) system with a gaussian frequency distribution, $g(\nu)$, given by:

$$g(\nu)=\frac{1}{\sqrt{2\pi\sigma^2}}\exp\left(-\frac{\nu^2}{2\sigma^2}\right) \tag{12}$$

where σ is the standard deviation of $g(\nu)$. For $g(\nu)$ in Eq. (12), the line width at half max is $\Delta\nu_{\frac{1}{2}}=\sqrt{8\mathrm{Ln}(2)}\sigma$. In Figure 5, simulations of low-power excitation using a constant pulse shape of fixed pulse length $T_p=5$ ms were performed for nominal flip-angles $\Theta=2\pi\nu_{RF}T_p=\frac{\pi}{6}$

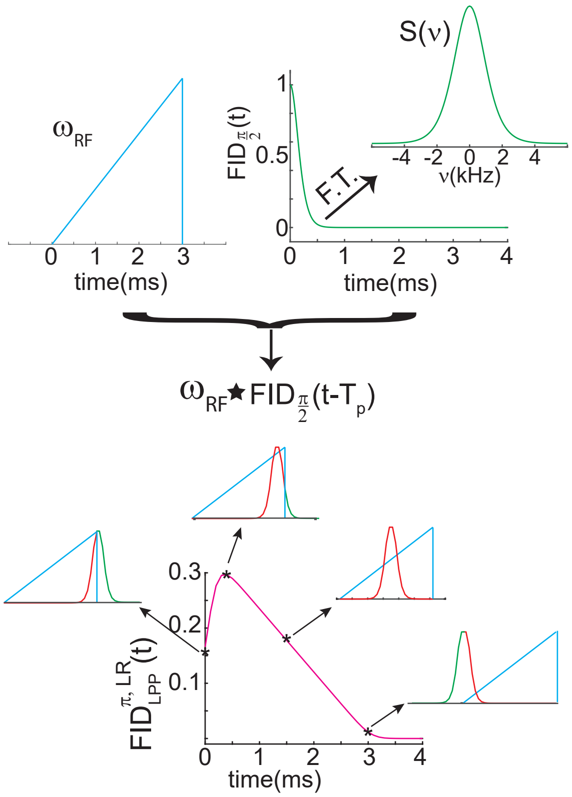

FIG. 4. The signal after low-power excitation followed by a π_X-pulse in the LR regime, $\mathrm{FID}^{\pi,LR}_{LPP}(t)$ [Eq. (11)], is given by the cross-correlation of the RF pulse shape, $\omega_{RF}(t)$ with the $\mathrm{FID}_{\frac{\pi}{2}Y}(t-T_p)$ in Eq. (10), i.e., $\mathrm{FID}^{\pi,LR}_{LPP}(t) = \omega_{RF}\star\mathrm{FID}_{\frac{\pi}{2}Y}(t-T_p)$. In this figure, a ramped pulse shape, $\omega_{RF}(t) = \frac{2\Theta t}{T_p^2}$ for $0 \leq t \leq T_p$ with $T_p = 3$ ms and $\Theta = \frac{\pi}{3}$. As illustrated, $\mathrm{FID}^{\pi,LR}_{LPP}(t)$ resembles the time-reversed RF pulse shape. The integrand in Eq. (11) is illustrated at times (denoted by '*') $t = 0$, $t = 0.4$ ms, $t = 1.5$ ms, and $t = T_p = 3$ ms, where red indicates the contribution of the $\mathrm{FID}_{\frac{\pi}{2}Y}(t)$ to the integrand in Eq. (11) and green indicates the portion of $\mathrm{FID}_{\frac{\pi}{2}Y}(t)$ that does not contribute.

[$\nu_{RF} \approx 16.7$ Hz], $\Theta = \frac{\pi}{3}$ [$\nu_{RF} \approx 33.3$ Hz] and $\Theta = \pi$ [$\nu_{RF} = 100$ Hz] on three different $g(\nu)$ given in Eq. (12): $\sigma = 80$ Hz [Fig. 5(A), $\Delta\nu_{\frac{1}{2}} = 188.4$ Hz], $\sigma = 150$ Hz [Fig. 5(B), $\Delta\nu_{\frac{1}{2}} = 353.2$], and $\sigma = 300$ Hz [Fig. 5(C), $\Delta\nu_{\frac{1}{2}} = 706.4$ Hz]. As the line width of $g(\nu)$ increased, $\mathrm{FID}^{\pi}_{LPP}(t)$ became more "box-like" for $\Theta = \frac{\pi}{6}$ and $\Theta = \frac{\pi}{3}$. For $\Theta = \pi$, a sharper edge to $\mathrm{FID}^{\pi}_{LPP}(t)$ at $t \approx T_p$ occurred when $\Delta\nu_{\frac{1}{2}} > 3\nu_{RF}$ as seen in Fig. 5(C). Furthermore, the maximum intensity of $\mathrm{FID}^{\pi}_{LPP}(t)$ near $t \approx T_p$ for $\Theta = \pi$ became larger than the intensity for either $\Theta = \frac{\pi}{6}$ and $\Theta = \frac{\pi}{3}$ when $\Delta\nu_{\frac{1}{2}} > 3\nu_{RF}$ [Fig. 5(C)], whereas it was roughly equal [Fig. 5(B)] or smaller [Fig. 5(A)] as $\Delta\nu_{\frac{1}{2}}$ decreased. With regards to Figure 11 in the main text where the various $\mathrm{FID}^{\pi}_{LPP}(t)$ observed for powdered and

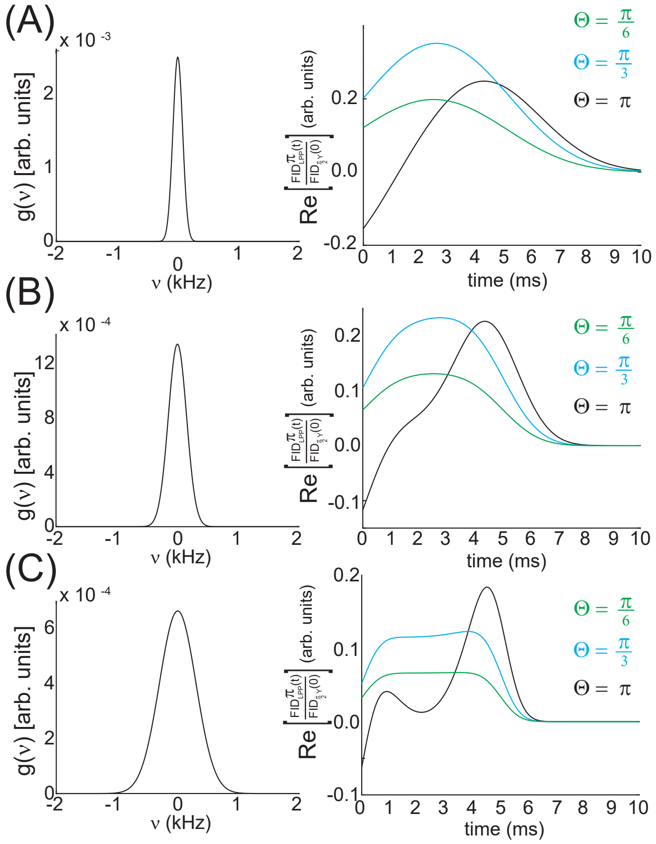

FIG. 5. Simulations of $\mathrm{FID}^{\pi}_{LPP}(t)$ for low-power excitation by a constant pulse shape of fixed length $T_p = 5$ ms in an inhomogeneously broadened spin system with a gaussian frequency distribution $g(\nu)$ given in Eq. (12) for three different σ, (A) $\sigma = 80$ Hz [$\Delta\nu_{\frac{1}{2}} = 188.4$ Hz], (B) $\sigma = 150$ Hz [$\Delta\nu_{\frac{1}{2}} = 353.2$ Hz], and (C) $\sigma = 300$ Hz [$\Delta\nu_{\frac{1}{2}} = 706.4$ Hz] and for three different Θ, $\Theta \in \left\{\frac{\pi}{6}, \frac{\pi}{3}, \pi\right\}$. When compared to the experimental $\mathrm{FID}^{\pi}_{LPP}(t)$ observed in single-crystalline and powdered adamantane and ferrocene shown in Fig. 11 of the main text, the results seem similar to those in (C) (indicating that the inhomogeneous broadening was much larger than the applied ν_{RF}). In all simulations, $\Delta t = 10\,\mu$s, $N_{pts} = 1000$, and the frequency range $\nu \in [-5000\,\mathrm{Hz}, 5000\,\mathrm{Hz}]$ was uniformly divided into $N_{div} + 1 = 20001$ spectral divisions with the frequency of the n^{th} division for $n \in \{0, 1, \ldots, N_{div}\}$ given by $\nu_n = -5000\,\mathrm{Hz} + n\delta\nu$ with $\delta\nu = \frac{10000}{20000}\,\mathrm{Hz} = 0.5$ Hz.

single-crystalline adamantane and ferrocene were presented, the behavior of $\mathrm{FID}^{\pi}_{LPP}(t)$ near $t \approx T_p$ was more similar to the behavior shown in Fig. 5(C), which suggests that the inhomogeneous broadening in those samples was larger than the applied ν_{RF}.

V. LOW-POWER EXCITATION FOR FIXED ν_{RF} IN POWDERED HEXAMETHYLBENZENE AT 400 MHZ FIELD STRENGTH

Experimental results for low-power excitation of powdered hexamethylbenzene, performed on a 400 MHz Bruker Avance III NMR spectrometer equipped with a PA BBO 400S1 BBF-H-D-05-Z-SP-FB probe, are shown in Figure 6. In this experiment, shimming on a D_2O sample was not performed prior to the solid-state experiments (as was done for the experiments presented in the main text). However, the results were still similar to those shown in Figure 10 in the main text on powdered hexamethylbenzene observed at 500 MHz field strength. Nonzero signal was obtained for both $\mathrm{FID}_{LPP}(t)$ and $\mathrm{FID}^{\pi}_{LPP}(t)$, yet again indicating that nonzero chemical shift differences are not required to observe these long-lived signals in dipolar solids. While $\mathrm{FID}^{\pi}_{LPP}(t)$ and the corresponding spectra were similar at both 400 MHz and 500 MHz field strengths, $\mathrm{FID}_{LPP}(t)$ and the corresponding spectra for $\Theta = \frac{\pi}{3}$ and $\Theta = \frac{\pi}{6}$ showed some differences, particularly the "peak" near $\nu \approx 0$ Hz. This "peak" observed in hexamethylbenzene for $\Theta \leq \frac{\pi}{3}$ is somewhat reminiscent of the "peak" near $\nu \approx 0$ Hz seen in Figs. 2(A) and 2(C) in the linear spin chain simulations for $\Theta \leq \frac{\pi}{3}$. As discussed in the main text, whether a "peak" or a "dip" is observed at $\nu \approx 0$ Hz under low-power excitation depends upon the distribution of transition frequencies $\nu^{m,m-1}_{k,j}$ and whether enough destructive interference can occur to generate a "dip". For $\Theta = \frac{\pi}{2}$ and $\Theta = \pi$, the spectra under low-power excitation were similar at both 400 MHz and 500 MHz field strengths.

VI. PULSE PROGRAMS

Basic pulse program for low-power excitation

(gron0 is switching gradient on; sp1 is low-power shape pulse; d2 is delay before acquisition)

```
1 ze
  300u
2 d1
  300m gron0
  (p1:sp1 ph1):f1
  d2
  go=2 ph31
  wr #0
```

```
  100m groff
3 exit

ph1=0 2 2 0 1 3 3 1
ph31=0 2 2 0 1 3 3 1
```

Basic pulse program for low-power excitation followed by a π pulse

(gron0 is switching gradient on; sp1 is low-power shape pulse; d2 and d3 are necessary delays for power switching; d4 is delay before acquisition)

```
1 ze
  300u
2 d1
  300m gron0
  (p1:sp1 ph1):f1
  d2
  d3 pl2:f1
  p2 ph2
  d4
  go=2 ph31
  wr #0
  100m groff
3 100u
  exit

ph1=0 2 2 0 1 3 3 1
ph2=1 1 3 3 2 2 0 0
ph31=0 2 2 0 1 3 3 1
```

---

[1] Gong, Z. & Walls, J. D. Breakdown of linear response theory under low-power excitation in NMR. I: The case of long-lived signals in inhomogeneously broadened spin systems. *J. Chem. Phys.* **145**, 164201 (2016).

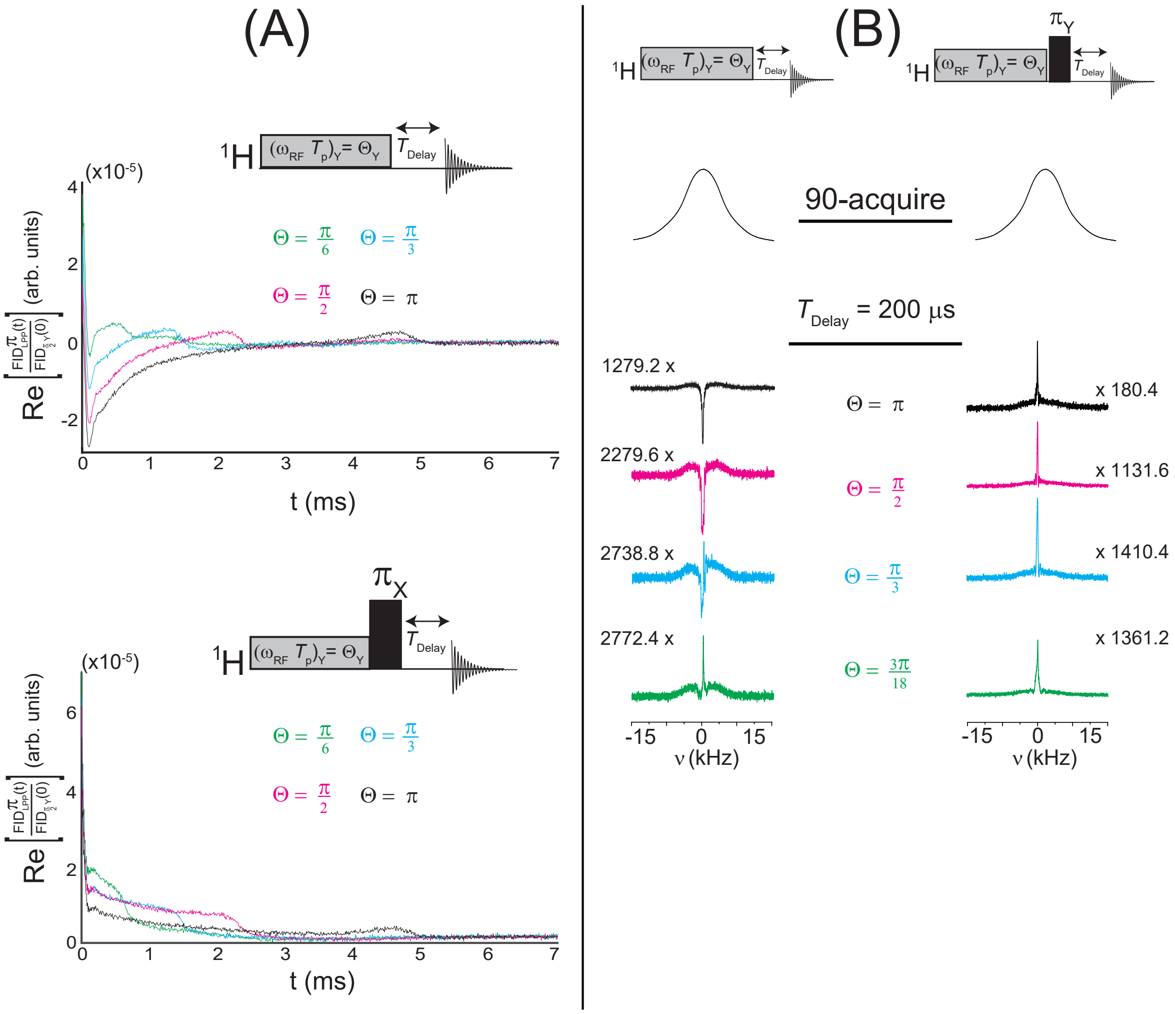

FIG. 6. Experimental (A) FIDs and (B) spectra for low-power RF excitation using a constant pulse shape ($\nu_{RF}(t) = \nu_{RF}$ for $0 \leq t \leq T_p$ with $\nu_{RF} = 100$ Hz) in powdered hexamethylbenzene on an AVANCE III HD 400 MHz Bruker spectrometer. The RF strength for the hard $\frac{\pi}{2}$- and π-pulses was ν_{RF} = 29.41 kHz. Low-power excitation spectra were acquired for nominal flip-angles of $\Theta = 2\pi\nu_{RF}T_p \in \left\{\frac{\pi}{6}, \frac{\pi}{3}, \pi\right\}$. All experiments were acquired with a dwell time $\Delta t = 8.4\,\mu$s, $N_{pts} = 11834$ complex data points, 4096 scans for the low-power excitation (only 16 scans were necessary for the $\frac{\pi}{2}$-acquire experiments), and a relaxation delay of $d_1 = 5$ s (T$_1$ was estimated to be $T_1 \approx 0.83$ s). An acquisition delay of $T_{\text{Delay}} = 200\,\mu$s was used in all experiments. Scaling factors with respect to the $\frac{\pi}{2}$-acquire spectra are shown next to each spectrum (the scale was estimated based on the assumption that the receiver gain was linear).